Exploring the Conformational Space of Chromatin Fibers and Their Stability by Numerical Dynamic Phase Diagrams

René Stehr,[†] Robert Schöpflin,[†] Ramona Ettig,[‡] Nick Kepper,[‡] Karsten Rippe,[‡] and Gero Wedemann[†*]
[†]University of Applied Sciences Stralsund, System Engineering and Information Management, Stralsund, Germany; and [‡]Deutsches Krebsforschungszentrum and BioQuant, Research Group Genome Organization and Function, Heidelberg, Germany

ABSTRACT The three-dimensional structure of chromatin affects DNA accessibility and is therefore a key regulator of gene expression. However, the path of the DNA between consecutive nucleosomes, and the resulting chromatin fiber organization remain controversial. The conformational space available for the folding of the nucleosome chain has been analytically described by phase diagrams with a two-angle model, which describes the chain trajectory by a DNA entry-exit angle at the nucleosome and a torsion angle between consecutive nucleosomes. Here, a novel type of numerical phase diagrams is introduced that relates the geometric phase space to the energy associated with a given chromatin conformation. The resulting phase diagrams revealed differences in the energy landscape that reflect the probability of a given conformation to form in thermal equilibrium. Furthermore, we investigated the effects of entropy and additional degrees of freedom in the dynamic phase diagrams by performing Monte Carlo simulations of the initial chain trajectories. Using our approach, we were able to demonstrate that conformations that initially were geometrically impossible could evolve into energetically favorable states in thermal equilibrium due to DNA bending and torsion. In addition, dynamic phase diagrams were applied to identify chromatin fibers that reflect certain experimentally determined features.

INTRODUCTION

In eukaryotic cell nuclei, DNA is wrapped 1.67 times around a histone octamer protein core. The resulting protein-DNA complex is referred to as the nucleosome and represents the basic building block of chromatin (1). Nucleosomes are connected via the intervening linker DNA and form a beads-on-a-string-like structure that can associate into a chromatin fiber (1,2). In addition, the H1 linker histone or the variant linker histone H5 found in avian erythrocytes can bind to the nucleosome. The resulting structure is termed a chromatosome and can promote the further compaction to the chromatin fiber structure (1,3,4). The spatial organization of nucleosomes in the chromatin fiber affects DNA accessibility and is therefore an important factor in processes such as transcription, replication, repair, and recombination (3,5–7). Although the structure of the nucleosome is known at atomic resolution (8), the chromatin fiber structure and its higher-order organization remain controversial and various models have been suggested (1,3,9,10). Two types of models can be distinguished: solenoid models, in which consecutive nucleosomes on the chain stack on each other to form a helical fiber structure (11), and crossed-linker models with straight linker DNA that mediate contacts between nucleosomes that are not directly adjacent on the nucleosome chain (12). The available experimental data point to the existence of different chromatin fiber geometries. Numerous structures have been proposed, including 1), a crossed-linker two-start helix without linker histone based on the crystal structure of a tetranucleosome particle (13); 2), a one-start helix with interdigitated (ID) nucleosomes as derived from electron microscopy studies of reconstituted chromatin fibers (14,15); and 3), a two-start helix conformation with crossed-linker DNA and a zig-zag-like DNA backbone with a so-called nucleosome stem motif, which occurs for native chromatin of chicken erythrocytes (16,17).

To explore the conformational space of the nucleosome chain, investigators have used Monte Carlo (MC) simulations to gain valuable insights into the structure of chromatin in thermal equilibrium (18–25). To include additional degrees of freedom for the folding of the nucleosome chain and allow investigation of structures that are not accessible in the two-angle model, a six-angle model for the nucleosome geometry in the fiber was recently introduced (25). However, for a number of experimental findings, such as those obtained with reconstituted chromatin with $\geq$207 basepair (bp) nucleosome repeat lengths (NRLs), model structures are still lacking (4,15,20). High-resolution experimental data for the nucleosome/chromatosome geometry with respect to the path of the incoming and outgoing DNA are currently limited to that of the tetranucleosome crystal structure with 167 bp NRL. In addition, the dependence of the fiber structure on the salt concentration (22,26–28) as well as on other factors, such as the (cooperative) binding of linker histones (16,17,29,30), need to be investigated further.

In a simplified description termed the ''two-angle model'', the conformation of the nucleosome chain with a given NRL is described by a torsion angle β between nucleosomes and a DNA entry-exit angle α at the nucleosome (31). This model has been used to investigate the large number of geometrically possible nucleosome geometries in phase diagrams (32–35). In these diagrams, properties of the chromatin fiber

Submitted May 10, 2009, and accepted for publication November 24, 2009.

*Correspondence: Gero.Wedemann@fh-stralsund.de

Editor: Gregory A. Voth.

0006-3495/10/03/1028/10 $2.00

doi: 10.1016/j.bpj.2009.11.040

were analyzed in a two-dimensional parameter space defined by the angles α and β, with a focus on the geometrically possible conformations and their properties, e.g., their energy (36). However, there are several fiber conformations, such as those based on the tetranucleosome crystal structure or the fibers proposed for chromatin from chicken erythrocytes (20,25), that are stable in thermal equilibrium but can only form after considerable DNA bending and twisting to obtain an energetically favorable stacking of two nucleosomes. With relaxed DNA, these fibers would be classified as sterically impossible in the two-angle phase diagrams. Here, phase diagrams and MC simulations were combined to take advantage of both approaches. First, numerical phase diagrams for the energy associated with a given chromatin fiber were developed. In contrast to phase diagrams of the two-angle model (32–35), more complex nucleosome geometries according to the six-angle model were considered and the associated energies were calculated. The resulting phase diagrams revealed considerable energy differences between the fiber geometries. Subsequently, their stability was evaluated in MC simulations. This novel approach accounts for energetic and entropic effects on chromatin fiber compaction, and is referred to as a numerical dynamic phase diagram (DPD). It was applied to identify chromatin structures, which are in better agreement with the available experimental data than previously proposed model structures (20,25).

MATERIALS AND METHODS

Six-angle chromatin computer model and MC simulations

Numerical phase diagrams were created based on the six-angle computer model of chromatin (20,21,25). In this model, nucleosomes are represented by a spherocylindrically shaped potential that interacts between different nucleosomes. The nucleosomes are connected via linker DNA segments (Fig. 1 *A*). The two-angle model (31) is extended by additional degrees of freedom to account for certain nucleosome and chromatosome geometries (20). The actual opening angle, here denoted as ψ, is determined by the entry-exit angles α and γ measured parallel and perpendicular to the flat side of the nucleosome cylinder, respectively (Fig. 1 *A*). The energy of the system is a sum of different contributions as described previously (20,21,25). These comprise 1), the elastic properties of DNA modeled by harmonic potentials for stretching, torsion, and bending; 2), the electrostatic repulsion of the DNA described by a Debye-Hückel approximation and parameterized for a salt concentration of 100 mM NaCl; 3), the nucleosome-nucleosome interaction potential calculated from a series expansion

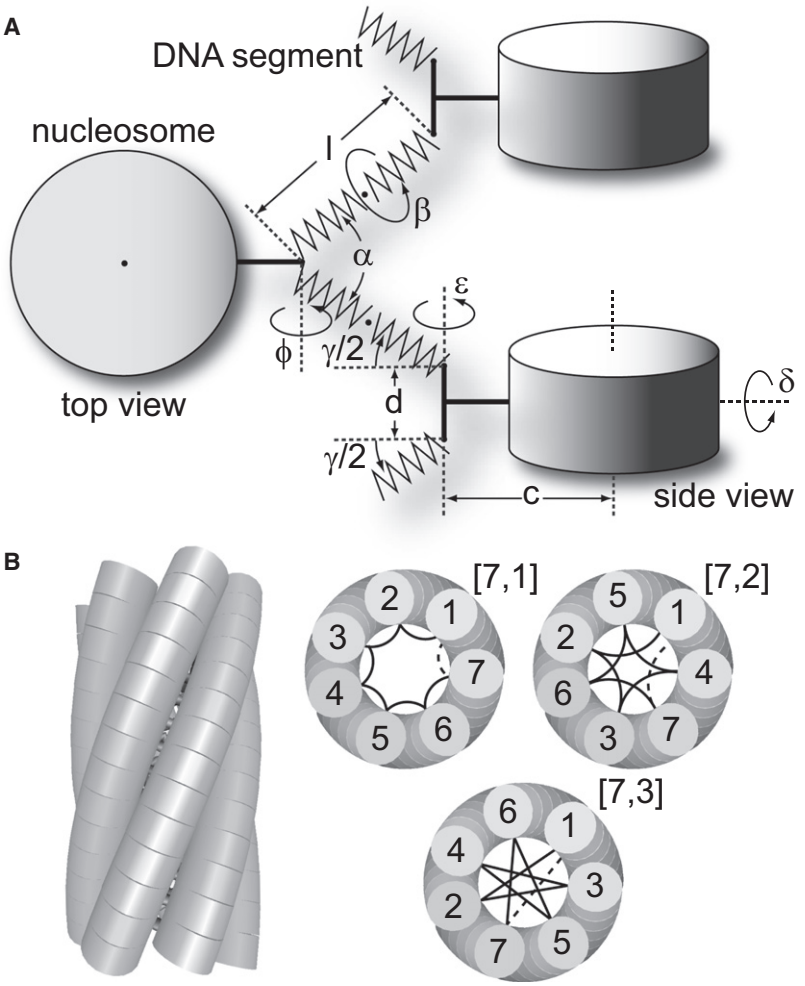

FIGURE 1 (*A*) Schematic description of the six-angle model of chromatin. The nucleosomes are connected by pieces of elastic DNA with length l (depicted as springs). The nucleosomes are shown as cylinders; however, they are represented by an anisotropic potential as spherocylindrical particles. The angles α, γ, and β describe the DNA path between consecutive nucleosomes, and ϕ, ε, and δ describe the nucleosome orientation relative to the incoming and outgoing linker DNA. The parameter c is the distance from the center of the histone core to the start of the linker DNA and can describe a nucleosome stem structure (16,17). The gap between the two DNA strands leaving and entering the chromatosome core particle at this point is denoted by d. For more details, see the Supporting Material. (*B*) Denotation of the chromatin fiber structures by nucleosome stacks and DNA path according to Depken and Schiessel (37). A sample fiber structure is shown (left: side view, right: top view). A helical winding of the chain is described by $[N_{stack}, N_{step}]$, where N_{stack} is the number of nucleosome stacks and N_{step} is the step size across stacks between connected nucleosomes. A seven-start helix with different linker DNA paths (*black lines*) is shown with solenoidal ([7, 1]) and crossed-linker DNA ([7, 2] and [7, 3]) paths. The dashed line marks the linker DNA to the nucleosome of the next turn.

in S-functions; and 4), the excluded volume between DNA segments and nucleosomes described by a soft core repulsive potential. A detailed description of the six-angle model and all energy terms is given in the Supporting Material, and the simulation parameters are listed in Table S1.

A given chromatin fiber structure is referenced by the denotation introduced by Depken and Schiessel (37). The folding of the nucleosome chain is described by two parameters $[N_{stack}, N_{step}]$, where N_{stack} (corresponding to N_{rib} in Depken and Schiessel (37)) is the number of top-on-top nucleosome stacks, and N_{step} is the step size between connected nucleosome stacks (Fig. 1 *B*). For example, the solenoid model is described by [1, 1], two-start fibers by [2, 1], and ID fiber models with various numbers of nucleosome stacks n by $[n, 1]$ with $n > 2$. Fiber models with crossed-linker DNA are characterized by higher step numbers N_{step}, e.g., a five-start helix [5, 2] or seven-start helix [7, 3] (Fig. 1 *B*). Chromatin fibers with irregular or no stacking of nucleosomes cannot be represented by this denotation.

For the computation of numerical DPDs, MC simulations were conducted. A Metropolis MC algorithm with rotation and pivot moves was used (21,25). Selected structures were subjected to extended simulations to achieve a representative sample of conformations in thermal equilibrium. The number of simulation steps was chosen such that at least 200 statistically uncorrelated conformations were generated. For the phase diagrams, structures were parameterized to have a maximal nucleosome-nucleosome attraction energy E_{max} of 6 k_BT. Additional simulations were conducted with E_{max} of 9 and 12 k_BT with a replica exchange procedure, with up to 160 replicas used to avoid trapping into local energy minima (25).

Chromatin fiber models

Phase diagrams were investigated for three different nucleosome geometries selected from recent studies (Fig. S1 and Table S2 of the Supporting Material): 1), the crossed-linker (CL) two-start helix geometry derived from the tetranucleosome crystal structure with an NRL of 169 bp (13,20); 2), a crossed-linker model with a nucleosome stem structure (CLS), where the stem size represents the conformation introduced by binding of the linker histone H5. This model was parameterized to fit the data of native chromatin of chicken erythrocytes with an NRL of 212 bp (21,25); and 3), the ID geometry model, which represents a model for reconstituted chromatin in the presence of linker histones with high mass densities for NRLs of 187, 197, and 207 bp (15,20). The CLS geometry can be described by the two-angle model (31), whereas the CL and ID models require the six-angle model (20).

Numerical phase diagrams

Numerical phase diagrams of chains with 100 nucleosomes were examined for the opening angle ψ as a function of α and γ, and the nucleosome twist angle β. For the static phase diagrams, the continuous two-dimensional space was divided into steps of 1° in the range of 0–180° and 0–359° for ψ and β, respectively. For smaller ranges of ψ, steps of 0.5° were used. The remaining parameters of the six-angle model were kept at the values of the respective model (Table S2). In the static phase diagrams, all chromatin conformations were considered to be fully relaxed in terms of the elastic DNA potentials for bending, torsion, and stretching. Thus, in the initial conformations, the DNA elastic energies made no contribution to the total energy. Only energy terms for the electrostatic interaction between the linker DNA, the internucleosomal interaction, and the DNA-nucleosome excluded volume potential contributed to the total energy. A threshold of 1000 k_BT for the total energy was chosen to distinguish between sterically possible and impossible conformations. Phase diagrams were also created to visualize the energy associated with a given fiber conformation.

For each configuration of the DPDs, an MC simulation with 10^7 simulation steps was performed. Chromatin structures were evaluated in terms of the energies determined for the last conformation of the simulated trajectory. Furthermore, experimentally accessible properties such as diameter, linear mass density, and fiber shape, as described previously (25), were systematically investigated. To reduce computing time, the step width of the raster in the DPDs was enlarged by a factor of 5.

RESULTS

The static phase diagram of the CLS model reveals stability differences between chromatin fiber conformations

Corresponding to previous investigations of the CLS geometry (18,21,25), the opening angle ψ was chosen to fulfill the condition $\gamma = 0$ and $\psi = \alpha$, so that the phase diagram could be compared with previous phase diagrams of the two-angle model (32–35) (Fig. 2 *A*). The result is depicted in Fig. 2 *B*. In some regions, especially at the border between sterically possible and impossible conformations, the energies were significantly above average. This is caused by the electrostatic repulsion of linker DNA in close proximity (Fig. S2 *A*). In particular, conformations with more than three nucleosome stacks and a crossed-linker DNA path exhibited high electrostatic energies, e.g., [5, 2] and [7, 3] fibers (Fig. 2 *B*, fibers 5 and 7). The low-energy regions were usually

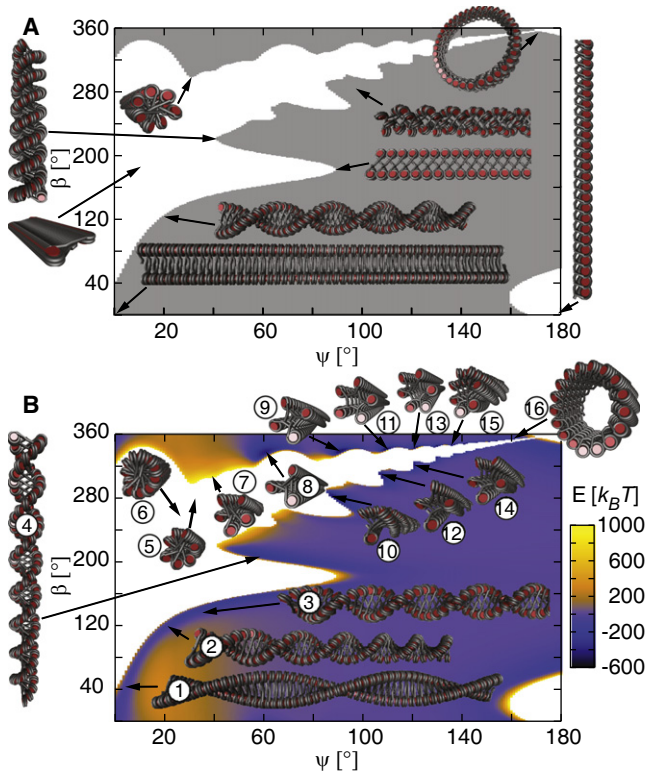

FIGURE 2 Static energy phase diagrams of the CLS geometry with NRL = 212 bp for the opening angle ψ ($\gamma = 0$) and the nucleosome twist angle β with a step width of 1°. Fiber conformations with sterical overlaps are represented in white. (*A*) A classical phase diagram representation in which the region of fiber conformations without sterical overlaps is depicted in gray. (*B*) A phase diagram showing the energy E associated with a given fiber conformation. The diagram exhibits regions of very high energy caused by electrostatic DNA repulsion. These include fibers with crossed-linker DNA, e.g., [5, 2], [11, 5] and [7, 3] (fibers 5–7). In contrast, [2, 1] zig-zag fiber conformations (fibers 1–4) and [3, 1] and [4, 1] fibers (fibers 8–10) have the broadest energy valleys, whereas $[n, 1]$ structures with $n > 4$ exhibit lower energy values but smaller valleys (fibers 11–16). Fiber 6 represents our previous model of chromatin from chicken erythrocytes (25).

associated with a favorable nucleosome-nucleosome attraction term (Fig. S2 *B*). In addition to nucleosome stacking, optimal lateral orientation of two nucleosomes can yield significant attraction energy (25). Accordingly, interdigitated [*n*, 1] conformations with $n > 4$ and closely arranged nucleosome stacks led to the lowest energy (Fig. 2 *B*, fibers 11–16). The [2, 1] zig-zag (Fig. 2 *B*, fibers 1–4) and interdigitated [3, 1] and [4, 1] (Fig. 2 *B*, fibers 8–10) fibers displayed the broadest energy valleys. It is noted that a recently developed model for chromatin of chicken erythrocytes (25) is located in the sterically forbidden area in the absence of DNA bending/twisting (Fig. 2 *B*, fiber 6).

The energy landscape of the static phase diagram depends strongly on the nucleosome geometry

Energy phase diagrams were also created for the CL and ID models. For the CL geometry, the condition $\gamma = -\alpha$ was used, which corresponds to the tetranucleosome model structure (20). The resulting energy phase diagram differed significantly from the CLS model with respect to the shape of the sterically forbidden region and energy values (Fig. 3 *A*). Two-start helix conformations ([2, 1] fibers) displayed the deepest and broadest energy valley (Fig. 3 *A*, fibers 1–4) but were also found to be associated with high energies (Fig. 3 *A*, fibers 5 and 6). Furthermore, conformations with an increased number of nucleosome stacks (e.g., [4, 1], [5, 1], and [8, 1] fibers (Fig. 3 *A*, fibers 7–10)) were present, but were not located within the low-energy valleys.

For the ID geometry, α was set to the previously selected value of 117.5° (20), and γ was varied to obtain the opening angle ψ plotted in the phase diagram. For an NRL of 187 bp, broad low-energy valleys were apparent (Fig. S3 *A*). Notably, for 197 bp (Fig. 3 *B*) and in particular for 207 bp (Fig. S3 *B*), these regions disappeared. In all diagrams for the ID geometry, the low-energy regions were present near the border that separates sterically possible and impossible conformations (Fig. 3 *B* and Fig. S3). These were [*n*, 1] fibers with $n > 4$, which are energetically advantageous due to the high number of nucleosome stacks. For the CL (Fig. 3 *A*, fiber 5) and ID geometry with NRLs of 187 (Fig. S3 *A*, fiber 2) and 207 bp (Fig. S3 *B*, fiber 1), the states of the previous developed models (20) were found to be located in sterically forbidden areas, since DNA deformations to avoid clashing of nucleosomes were not allowed in the static phase diagrams.

Sterically impossible conformations can be transformed into energetically favorable ones by DNA bending and twisting

A subset of conformations of the static phase diagrams was simulated for 10^7 MC steps to create DPDs. During the simulation, fiber conformations changed due to DNA bending and twisting. The resulting phase diagrams differed considerably from the static ones. Most of the initially forbidden areas

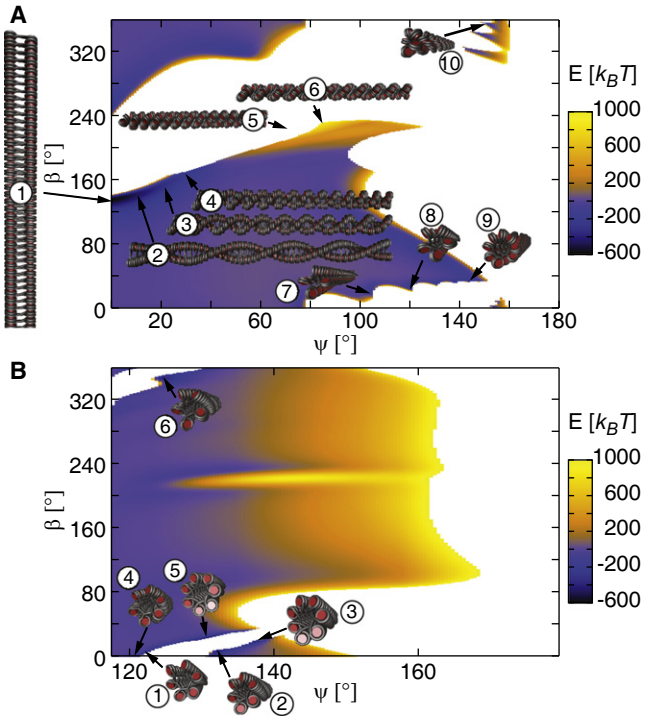

FIGURE 3 Static energy phase diagrams of different nucleosome geometries for the opening angle ψ and the nucleosome twist angle β. (*A*) CL geometry with NRL = 169 bp. The step width for ψ and β is 1° and the opening angle ψ results from the condition $\gamma = -\alpha$. A broad energy valley exists for [2, 1] conformations (fibers 1–4). More compact [*n*, 1] fibers with $n > 4$ exhibit no apparent energy valleys (fibers 7–10). Fiber 5 is our previous model based on the tetranucleosome crystal structure (20). (*B*) ID geometry with NRL = 197 bp. The angle α was set to 117.5°, and γ was varied to achieve the actual angle ψ. Step widths of 0.5° and 1° were used for ψ and β, respectively. Most of the sterically possible regions in the diagram with large opening angles led to high energies. The [5, 1], [6, 1], and [7, 1] fibers with opening angles between 120° and 140°, and twist angles < 40° yielded the lowest energy (fibers 1–3, 5, and 6). Fiber 4 is the previously derived model for chromatin fibers reconstituted on arrays of strong nucleosome positioning elements (20).

became populated (Fig. 4 and Fig. S4). For the CLS geometry, [*n*, 1] fiber conformations with $n > 3$ led to the lowest energy (Fig. 4 *A*, fibers 5, 6, 8, and 9). However, [2, 1] and [3, 1] fiber conformations were also energetically favorable (Fig. 4 *A*, fibers 1–4 and 7). The CL geometry retained the initial [2, 1] type fibers as the most favorable conformation but became slightly more irregular and less dense (Fig. 4 *B*). For the ID geometry with an NRL of 197 bp, a large low-energy region with mostly [6, 1] and [7, 1] fiber conformations appeared (Fig. 4 *C*). For an NRL of 187 bp, the DPD yielded extended low-energy regions for [5, 1] and [6, 1] fiber conformations (Fig. S4 *A*). For an NRL of 207 bp, only [*n*, 1] fiber conformations with $n > 11$ and large diameters (>47 nm) retained their fiber-like shape (Fig. S4 *B*). In general, the energetically most favorable regions occurred near the border between previously sterically possible and impossible conformations in the DPDs of the different fiber types.

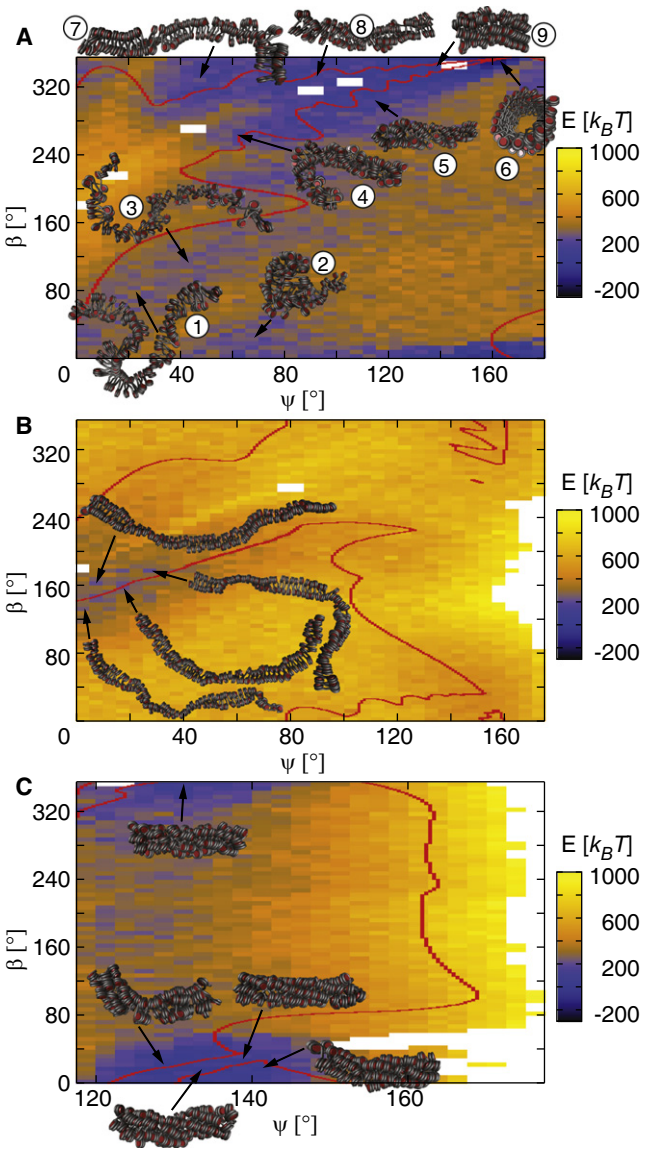

FIGURE 4 Dynamic energy phase diagrams for the opening angle ψ and the nucleosome twist angle β (corresponding to Figs. 2 and 3). The red contour lines indicate the former borderline between sterically possible and impossible conformations of static phase diagrams (Figs. 2 and 3). Chromatin structures became more irregular. Most of the conformations that initially were sterically forbidden became possible and, in part, even energetically favorable. (*A*) CLS geometry with NRL = 212 bp. Structures that were initially located in regions of low energy mostly retained their shape (fibers 1, 3, 5, 6, 8, and 9). Fiber structures with more than four nucleosome stacks and crossed-linker DNA, e.g., [5, 2], [7, 3] and [11, 5] (Fig. 2 *B*, fibers 5–7), transformed to [3, 1] fibers (fibers 4 and 7). (*B*) CL geometry with NRL = 169 bp. The initially existing energy valley broadened, with [2, 1] fibers being the energetically most favorable conformations. The [*n*, 1] fibers with $n > 4$ (Fig. 3 *A*, fibers 7–10) were unstable (data not shown). (*C*) ID geometry with NRL = 197 bp. The [5, 1] and [6, 1] conformations retained their fiber-like structure and were the energetically most favorable.

For the CL geometry, the recently developed chromatin model based on the tetranucleosome crystal structure was initially located in the forbidden region of the phase diagram (Fig. 3 *A*, fiber 5) (20). This DPD was searched for energetically more favorable structures that satisfy the properties of the tetranucleosome structure. A [2, 1] fiber conformation ($\psi = 25°$, $\beta = 175°$) was found in a broad energy valley, which was further investigated in thermal equilibrium by extensive MC simulation (Fig. 5 *A*). Properties were computed as mean values from the resulting ensemble (Table 1). The newly identified structure had average values of 27.8 nm diameter, 2.9 nucleosomes/11 nm fiber linear mass density, and a 136 k_BT lower total energy than the previously constructed model (Table S3).

New stable ID fiber conformations were detected in the numerical phase diagram analysis

Recently developed models for the ID geometry were reevaluated to identify structures that were in better agreement with the experimental data from electron microscopy images of reconstituted chromatin. For NRLs of 187–207 bp, a diameter of ~33 nm and a linear mass density of ~11 nucleosomes/11 nm fiber were measured. Fibers with higher NRLs had ~44 nm diameter and a linear mass density of ~15 nucleosomes/11 nm (15). For an NRL of 187 bp, the DPD revealed two types of ID fiber conformations. The first type ($\psi = 117.5°$, $\beta = 295°$) contained nucleosomes with parallel alignment to the fiber axis (Fig. 5 *B*). However, in the other [6, 1] fiber ($\psi = 125°$, $\beta = 355°$), nucleosomes were stacked nearly perpendicular to the fiber axis (Fig. 5 *C*). Longer MC simulations revealed that both fiber-like structures were stable in thermal equilibrium, with a mean diameter of ~31 nm and mean linear mass densities of 7.1 ($\psi = 117.5°$, $\beta = 295°$) and 7.8 nucleosomes/11 nm fiber ($\psi = 125°$, $\beta = 355°$) (Table 1). For an NRL of 197 bp, a [7, 1] fiber ($\psi = 130$, $\beta = 355$) was the lowest-energy structure that agreed with the experimental data (Fig. 5 *D*). Long MC simulations of this conformation yielded a mean diameter of 35.9 nm and a mean linear mass density of 8.1 nucleosomes/11 nm fiber (Table 1).

A systematic search of the DPD computed for the ID geometry with 207 bp revealed that most of the fiber-like conformations with diameters between 30 and 40 nm were not stable in the simulation, whereas fibers with diameters > 47 nm were (Fig. S4 *B*, and data not shown). Thus, the static phase diagrams were used to identify structures with specific features derived from the experimental studies. Several of these fiber conformations showed an excellent agreement in terms of diameter and mass density (15). The conformations with the lowest energies were further investigated with higher E_{max} values by replica exchange simulations. The results indicated that fiber conformations with diameters < 40 nm were not stable even with E_{max} of 12 k_BT (data not shown). However, the conformation with $\psi = 133°$ and $\beta = 23°$ formed stable fiber conformations for E_{max} of 9 and 12 k_BT (Fig. 5 *E*). For $E_{max} = 9$ k_BT, the simulated trajectory exhibited different nucleosome stacking patterns: [7, 1], [8, 1] and [9, 1], which appeared, in part, in

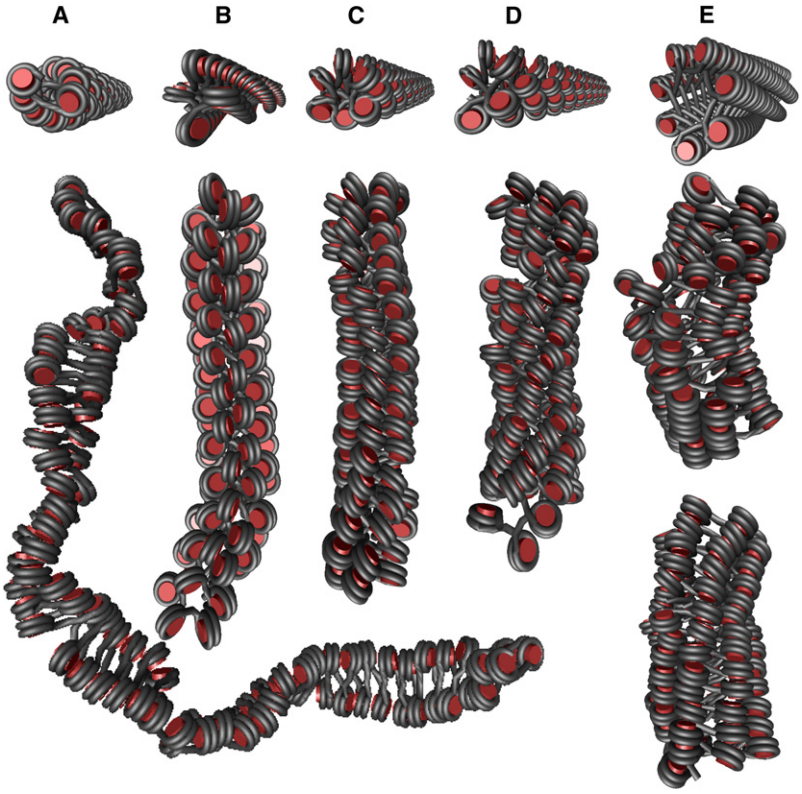

FIGURE 5 New structures for the CL and ID geometries derived from the numerical phase diagrams. The first row shows the initial structures as created in the static phase diagrams. The second row depicts sample fibers of the Boltzmann ensemble generated by extended MC simulations. The detailed properties of each structure are presented in Table 1. (*A*) CL geometry with 169 bp led to a [2, 1] fiber ($\psi = 25°$, $\beta = 175°$) with a mean diameter of 27.8 nm and a mean linear mass density of 2.9 nucleosomes/11 nm fiber. (*B*) ID fibers for NRL = 187 bp ($\psi = 117.5°$, $\beta = 295°$) with nucleosomes parallel to the chromatin fiber axis. The structure exhibits an open top-on-top stacking of nucleosomes with an average diameter of ~31 nm and mean linear mass density of 7.1 nucleosomes/11 nm fiber. (*C*) ID fibers for NRL = 187 bp ($\psi = 125°$, $\beta = 355°$) with nucleosomes nearly perpendicular to the chromatin fiber axis exhibits a [6, 1] fiber conformation. Average diameter and mass density were similar to the structure depicted in panel *B*. (*D*) ID fiber with NRL = 197 bp ($\psi = 130°$, $\beta = 355°$) yielded a [6, 1] fiber conformation with a mean diameter of 35.9 nm and a mean linear mass density of 8.1 nucleosomes/11 nm fiber. (*E*) ID fibers with NRL = 207 bp ($\psi = 133°$, $\beta = 23°$). The second and third rows show examples of a fiber simulated with E_{max} of 9 and 12 k_BT, respectively. For 9 k_BT, [7, 1], [8, 1], and [9, 1] fiber conformations (in part mixed within the chain) occurred, whereas for 12 k_BT more regular [7, 1] and [8, 1] fiber conformations appeared. Both structures had a mean diameter of ~45 nm and linear mass densities of 9.9 (9 k_BT) and 12.8 nucleosomes/11 nm fiber (12 k_BT).

a single fiber. For $E_{max} = 12\ k_BT$, more regular fibers with [7, 1] and [8, 1] stacking patterns were found. In some cases, the fiber started with seven stacks and ended with eight stacks. The structures had a diameter of ~45 nm and linear mass densities of 9.9 (9 k_BT) and 12.8 nucleosomes/11 nm fiber (12 k_BT) (Table 1).

DISCUSSION

Sterically possible chromatin fiber conformations

The static phase diagram for the CLS geometry (Fig. 2 *A*) reveals a variety of sterically possible structures. These include planar structures without nucleosome stacking, as well as zig-zag and interdigitated fibers, and depict a conformational space that is equivalent to that determined in analytical studies of the two-angle model (33,35). The shape of the forbidden region is similar to the phase diagram reported by Barbi et al. (32) even though the approach presented here is based on energy computation instead of geometric descriptions. In previous phase diagram investigations, it was concluded that the most compact fiber conformations exist at the border of the forbidden area (33,34), which is in agreement with the results presented here (Figs. 2 and 3, and Fig. S3). In contrast to previous phase diagram investigations (32–36), however, our numerical diagrams were computed with an increased conformation flexibility as given by the six-angle model. This allowed the systematic investigation of geometries that cannot be represented by the two-angle model but are of biological relevance, as discussed previously (20).

TABLE 1 New model structures derived from numerical phase diagrams further investigated by MC simulations

Geometry	NRL (bp)	ψ (°)	α (°)	γ (°)	β (°)	E_{max} (k_BT)	Fiber type [N_{stack}, N_{step}]	Diameter (nm)	Linear mass density (nucleosomes/11 nm fiber)
CL	169	25	17.7	−17.7	175	6	[2, 1]	27.8 ± 0.5	2.89 ± 0.06
ID	187	117.5	117.5	0	295	6	—	30.9 ± 0.15	7.1 ± 0.23
ID	187	125	117.5	−54.23	355	6	[6, 1]	31.3 ± 0.25	7.8 ± 0.25
ID	197	130	117.5	−70.89	355	6	[6, 1]	35.9 ± 0.7	8.1 ± 0.6
ID	207	133	117.5	−79.54	23	6	—	—	—
ID	207	133	117.5	−79.54	23	9	[7, 1], [8, 1], [9, 1]	45 ± 1.21	9.9 ± 1.25
ID	207	133	117.5	−79.54	23	12	[7, 1], [8, 1]	45.4 ± 0.42	12.8 ± 0.37

The remaining parameters of the six-angle model correspond to the values in Table S2. The values (mean and standard deviation) for the diameter and linear mass density were computed from the statistical ensemble in thermal equilibrium. The ID structure with $\psi = 117.5$ and $\beta = 295$ exhibited no distinct nucleosome stacking, and no fiber structure was achieved for the ID geometry with NRL = 207 bp and $E_{max} = 6\ k_BT$.

Energetically favorable chromatin fiber conformations

The static energy phase diagrams revealed a wide range of energetically unfavorable and favorable conformations (Figs. 2 and 3, and Fig. S3). Regions with high energy resulted mostly from electrostatic repulsion of linker DNA in close proximity, which is pronounced at the border between sterically possible and impossible conformations (Fig. S2 *A*). In contrast, regions of low electrostatic repulsion of linker DNA segments showed no specific location within the regions that defined a favorable conformation regime (Figs. 2 and 3, Fig. S2 *A*, and Fig. S3). This is in agreement with the results of different DNA repulsion energies in previously reported phase diagrams (33). Regions of low energy correlated with densely stacked nucleosomes (Fig. 2 *B* and Fig. S2 *B*), as previously found for the tetranucleosome crystal structure (13), electron microscopy images of reconstituted chromatin (15), and liquid crystals of nucleosome core particles (38).

As expected, the different nucleosome geometries had distinct low-energy conformations (Figs. 2 and 3, and Fig. S3). For the two-angle geometry of the CLS model, favorable [2, 1], [3, 1] and [4, 1] fiber conformations were found. Furthermore, [n, 1] fiber conformations with $n > 4$ (associated with larger fiber diameters) had lower energies but were located in narrower energy valleys, which are less favorable in terms of entropy. This type of interdigitated fiber was also found to be energetically most favorable for the ID geometry (Fig. 3 *B* and Fig. S3). Recently, similar fiber conformations were identified by a new geometric analysis based on the stacking of nucleosomes, which fit the experimental data mentioned above (37). Crossed-linker [5, 2] and [7, 3] fiber conformations were proposed to be more favorable than [5, 1], [7, 1], and [7, 2] fibers with bent linker DNA. In the analysis of the chromatin fiber stability conducted here, the crossed-linker fiber conformations with more than three nucleosome stacks (e.g., [5, 2] and [7, 3] fibers (Fig. 2 *B*, fibers 5 and 7)) were energetically unfavorable due to high electrostatic repulsion. These and similar crossed-linked fiber conformations were unstable during the simulations and changed to other conformations (see below). However, for [n, 1] fibers with $n > 4$, the nucleosome arrangement proposed by Depken and Schiessel (37) led to stable fiber conformations (Fig. 4, Fig. S3, and Fig. S4). Cooperative binding of H1 (4,29,30), binding of other architectural proteins such as HP1 (39), higher internucleosomal attraction (25,40), or different salt conditions (22,23,26–28) could stabilize conformations with crossed-linker DNA. Furthermore, straight and bent linker DNA may appear simultaneously in compacted chromatin fibers, as demonstrated in investigations of nucleosome interactions by cross-linking experiments and MC simulations (22).

In contrast to the CLS and ID geometries, the CL geometry favored [2, 1] two-start fiber conformations (Figs. 3 *A* and 4 *B*). This finding supports the previously proposed model in which the [2, 1] CL fibers represent chromatin fibers without linker histones, and the ID geometry represents the structure induced by binding of linker histones (20). This is in good agreement with experimental data of reconstituted chromatin fibers (4,15), the tetranucleosome crystal structure (13), and experimental data and computer simulations of oligonucleosomes with and without linker histones (22).

Chromatin fiber stability and ability to buffer local structure modifications

The DPDs revealed the stability of different fiber conformations. Crossed-linker fibers with more than three nucleosome stacks generally evolved into [3, 1] fibers (Fig. 4 *A*, fibers 4 and 7). This type of fiber was previously proposed as a model for chromatin of chicken erythrocytes (Fig. S1 *B*) (25). Furthermore, increased contacts between nucleosomes i and $i + 3$ appeared in part for compacted oligonucleosomes with linker histone and divalent cations investigated by cross-linking experiments and MC simulations (22).

The width of the energy valleys can serve as an indicator for the probability of fiber conformations because it reflects a favorable entropic contribution for the corresponding type of structures. In these regions, small changes in the nucleosome geometry, such as those induced by entropic effects, changes in salt concentration, or histone modifications, would lead only to small changes in the stability of the fiber. For instance, the [2, 1] fibers of the CL and CLS geometry were located in relatively broad energy valleys in the static phase diagrams (Figs. 2 *B*, fibers 1–4, and 3 *A*, fibers 1–4). The DPDs revealed that these fiber structures mostly retained their conformation in thermal equilibrium, but with a more irregular structure as compared to the initial states (Fig. 4 *A*, fibers 1 and 3, and Fig. 4 *B*). In contrast, conformations located in narrow energy valleys were limited in their conformational flexibility. Hence, they could represent states that are particularly responsive to regulatory changes that control the accessibility of the DNA for protein complexes involved in genome functions. For instance, the [n, 1] CLS conformations with $n > 3$ were located in a very narrow energy valley (Fig. 2 *B*, fibers 9–16). Even moderate differences of the opening angle and nucleosome twist angle would lead to considerable changes of these structures.

Due to entropic effects, all fiber conformations investigated became more irregular during the simulations (Fig. 4 and Fig. S4), which is in agreement with the behavior of native chromatin (41,42). Furthermore, fiber conformations that were sterically impossible with relaxed DNA in the initial structure transformed in many cases into energetically favorable states (Fig. 4 and Fig. S4). This behavior was most pronounced at the border, where energetically favorable fiber conformations were located. Structures with steric overlaps changed into those energetically more favorable states, which in turn required additional DNA bending and torsion.

In the set of simulations presented in Fig. 4 and Fig. S4, the DPDs were used to investigate the stability of the fiber conformations. Due to the limited number of MC simulation steps conducted for each structure, thermal equilibrium was reached only in some cases. However, 10^7 MC steps were sufficient to cause striking changes, e.g., from a sterically impossible [11, 5] to a favorable [3, 1] fiber conformation (Figs. 2 *B* and 4 *A*). Moreover, the extended simulation of the newly identified structures conducted here, as well as in our previous works, resulted in similar energy values as compared to the corresponding structures of the DPDs (Table S3). Thus, the simulated structures in the DPDs typically were close to thermal equilibrium after 10^7 MC steps. However, a reliable evaluation can only be made from additional simulations in which it is confirmed that thermal equilibrium has been reached.

Models for the tetranucleosome structure and reconstituted chromatin fibers

The newly identified [2, 1] fiber conformation for the CL geometry (Fig. 5 *A* and Table 1) is similar to the recently developed model based on the tetranucleosome crystal structure (Fig. S1 *A* and Table S2) in terms of the diameter and mass density (20). However, it has a significantly lower total energy due to reduced DNA bending and torsion. Both model structures are less compact than predicted from a simple repetition of the tetranucleosome crystal structure (13). This is in good agreement with electron microscopy images of reconstituted chromatin fibers without linker histones, which displayed very similar [2, 1] fibers (4).

For the ID geometry with an NRL of 187 bp, two possible fiber conformations were identified (Fig. 5, *B* and *C*, and Fig. S4 *A*): one with nucleosomes parallel (Fig. 5 *B*), and one with nucleosomes nearly perpendicular (Fig. 5 *C*) to the chromatin fiber axis (both with a mean diameter of 31 nm). The first is similar to the ID model of reconstituted chromatin that was recently proposed by Robinson et al. (15), whereas the latter [6, 1] fiber conformation corresponds to the proposed model of Daban and Bermúdez (14) and is similar to the recently reported model structures of Depken and Schiessel (37). The first model is in contrast to fibers with optimal stacking of nucleosomes (38), which served as the basis for various previously proposed models (14,37,43,44). MC simulations of similar ID fibers with parallel nucleosome orientation indicated that these structures were not stable in thermal equilibrium (20). Moreover, parallel and perpendicular nucleosome orientations with respect to the fiber axis were investigated for solenoid and zig-zag fibers by means of MC simulations (23). In comparison to parallel oriented nucleosomes, the perpendicular orientation resulted in a lower total energy with more realistic sedimentation coefficients. However, the apparent unfavorable parallel nucleosome orientation could be stabilized by additional linker histone interactions (4,29,30).

The MC simulations of conformations with NRLs $\geq$ 197 bp conducted here within the framework of the DPD analysis identified new stable fiber types (Fig. 5, *D* and *E*, and Table 1). For a 197 bp NRL, a [6, 1] fiber conformation with a mean diameter of 36 nm was found, which is in good agreement with experimental data (15). With an NRL of 207 bp, the mean diameter increased to ~45 nm, which corresponds to the experimental results for an NRL of 217 bp (15). However, these structures were less densely packed than those reported in experimental studies (4,15). Higher fiber compaction or smaller diameters could be induced by elevated internucleosomal interaction energies (25), cooperative binding of linker histones (4,29,30), or divalent cations (22) as used for the reconstitution of chromatin fibers (4,15). For an E_{max} of 6 k_BT, the DPDs for an NRL of 207 bp showed that most fiber-like conformations were not stable in the simulations. This is caused by high electrostatic repulsion of long DNA linkers and entropic effects, as observed in previous MC simulations (20,25). However, fiber conformations with an unrealistically high number of nucleosome stacks (>11) and large diameters (>47 nm) (Fig. S4 *B*) or with $E_{max} \geq 9\ k_BT$ (Fig. 5 *E* and Table 1) retained their fiber-like structures. It is therefore concluded that in reconstituted fibers with greater linker lengths, the maximum internucleosomal interaction energy E_{max} has to be at least 9 k_BT to overcome entropic and/or high electrostatic DNA repulsion forces. This agrees with the results of recent force spectroscopy experiments (N. Kepper, R. Ettig, R. Stehr, G. Wedemann and K. Rippe, unpublished results). Even higher interaction energies of 10–16 k_BT were inferred from a force spectroscopy study of reconstituted nucleosome arrays (40).

The new ID fiber type conformations identified here were more irregular than those proposed in previous studies (14,15,37,43). Of interest, stable fiber structures were found in different conformations (e.g., [7, 1] and [8, 1]) as well as in hybrid conformations that exhibited different nucleosome stacking patterns within a single chain of 100 nucleosomes. This points to a heterogeneity of fiber conformation that may be biologically relevant for establishing local variations of the structures associated with functionally different genomic elements.

CONCLUSIONS

The numerical phase diagrams introduced here provide a new approach for combining geometric and energetic aspects for systematic investigations of the folding of the nucleosome chain. The approach implemented in our DPD analysis closes the gap between static phase diagrams and MC simulations of single chromatin fibers. Energetically favorable and stable fiber conformations that reflect certain geometric features can be identified and then further investigated at thermal equilibrium by extended MC simulations. In general, comparisons of the static phase diagrams and DPDs

revealed that several unfavorable or sterically impossible fiber conformations evolved into energetically favorable states. Thus, computation of the DPDs allows for a more comprehensive exploration of the conformational space that is available for folding of the nucleosome chain than previously used approaches. Our results show that crossed-linker chromatin fibers with more than three nucleosome stacks were energetically unfavorable and unstable due to high electrostatic repulsion of linker DNA (Figs. 2 *B* and 4 *A*). Higher mass densities (>6 nucleosomes/11 nm fiber) were achieved with interdigitated fiber conformations. In addition, recently investigated model structures (20,25) were reevaluated to yield a better agreement with experimentally determined features (Fig. 5 and Table 1). A refined two-start helix fiber conformation (Fig. 5 *A*) was identified for chromatin without linker histone and low mass density with features that correspond to the tetranucleosome crystal structure (13). Furthermore, fiber conformations retrieved from the DPDs were in agreement with experimental data for reconstituted chromatin with fully saturated linker histone content (15). These include a fiber conformation with an NRL of 187 bp and nucleosomes oriented parallel to the fiber axis (Fig. 5 *B*). ID six-start helix fibers with nucleosomes perpendicular to the fiber axis were identified for NRLs of 187 (Fig. 5 *C*) and 197 bp (Fig. 5 *D*). For an NRL of 207 bp, corresponding seven- to nine-start helix fibers (Fig. 5 *E*) were found to adopt stable fiber conformation when the maximum internucleosomal interaction energy was at least 9 k_BT. Thus, for NRLs $\geq$ 197 bp, several new model structures were derived from the DPDs that extend the regime of stable fiber conformations as compared to that reported in our previous studies (20). In summary, the computation of DPDs allows one to investigate the many degrees of freedom of chromatin fiber conformations in relation to their stability in a systematic and comprehensive manner. This in turn makes it possible to identify conformations that satisfy experimentally determined criteria of interest, and to assign well-defined conformational states to the polymorphic nucleosome chain to elucidate its function as a dynamic regulator of DNA accessibility.

SUPPORTING MATERIAL

Supplementary methods, figures, and tables are available at http://www.biophysj.org/biophysj/supplemental/S0006-3495(09)05998-0.

This study was supported in part by the Volkswagen Foundation (New Conceptual Approaches to Modeling and Simulation of Complex Systems) and the Deutsche Forschungsgemeinschaft (grant Ri 1283/8-1 to K.R.). The simulations were conducted under project mvb00007 of the North German Supercomputing Alliance.

REFERENCES

1. van Holde, K. E. 1989. Chromatin. Springer, Heidelberg.
2. Woodcock, C. L., and S. Dimitrov. 2001. Higher-order structure of chromatin and chromosomes. *Curr. Opin. Genet. Dev.* 11:130–135.
3. Robinson, P. J., and D. Rhodes. 2006. Structure of the '30 nm' chromatin fibre: a key role for the linker histone. *Curr. Opin. Struct. Biol.* 16:336–343.
4. Routh, A., S. Sandin, and D. Rhodes. 2008. Nucleosome repeat length and linker histone stoichiometry determine chromatin fiber structure. *Proc. Natl. Acad. Sci. USA.* 105:8872–8877.
5. Henikoff, S. 2008. Nucleosome destabilization in the epigenetic regulation of gene expression. *Nat. Rev. Genet.* 9:15–26.
6. Tremethick, D. J. 2007. Higher-order structures of chromatin: the elusive 30 nm fiber. *Cell.* 128:651–654.
7. Wachsmuth, M., M. Caudron-Herger, and K. Rippe. 2008. Genome organization: balancing stability and plasticity. *Biochim. Biophys. Acta.* 1783:2061–2079.
8. Luger, K. 2006. Dynamic nucleosomes. *Chromosome Res.* 14:5–16.
9. Hansen, J. C. 2002. Conformational dynamics of the chromatin fiber in solution: determinants, mechanisms, and functions. *Annu. Rev. Biophys. Biomol. Struct.* 31:361–392.
10. Woodcock, C. L., A. I. Skoultchi, and Y. Fan. 2006. Role of linker histone in chromatin structure and function: H1 stoichiometry and nucleosome repeat length. *Chromosome Res.* 14:17–25.
11. Finch, J. T., and A. Klug. 1976. Solenoidal model for superstructure in chromatin. *Proc. Natl. Acad. Sci. USA.* 73:1897–1901.
12. van Holde, K., and J. Zlatanova. 1996. What determines the folding of the chromatin fiber? *Proc. Natl. Acad. Sci. USA.* 93:10548–10555.
13. Schalch, T., S. Duda, …, T. J. Richmond. 2005. X-ray structure of a tetranucleosome and its implications for the chromatin fibre. *Nature.* 436:138–141.
14. Daban, J. R., and A. Bermúdez. 1998. Interdigitated solenoid model for compact chromatin fibers. *Biochemistry.* 37:4299–4304.
15. Robinson, P. J. J., L. Fairall, …, D. Rhodes. 2006. EM measurements define the dimensions of the "30-nm" chromatin fiber: evidence for a compact, interdigitated structure. *Proc. Natl. Acad. Sci. USA.* 103: 6506–6511.
16. Bednar, J., R. A. Horowitz, …, C. L. Woodcock. 1998. Nucleosomes, linker DNA, and linker histone form a unique structural motif that directs the higher-order folding and compaction of chromatin. *Proc. Natl. Acad. Sci. USA.* 95:14173–14178.
17. Hamiche, A., P. Schultz, …, A. Prunell. 1996. Linker histone-dependent DNA structure in linear mononucleosomes. *J. Mol. Biol.* 257: 30–42.
18. Aumann, F., F. Lankas, …, J. Langowski. 2006. Monte Carlo simulation of chromatin stretching. *Phys. Rev. E Stat. Nonlin. Soft Matter Phys.* 73:041927.
19. Katritch, V., C. Bustamante, and W. K. Olson. 2000. Pulling chromatin fibers: computer simulations of direct physical micromanipulations. *J. Mol. Biol.* 295:29–40.
20. Kepper, N., D. Foethke, …, K. Rippe. 2008. Nucleosome geometry and internucleosomal interactions control the chromatin fiber conformation. *Biophys. J.* 95:3692–3705.
21. Wedemann, G., and J. Langowski. 2002. Computer simulation of the 30-nanometer chromatin fiber. *Biophys. J.* 82:2847–2859.
22. Grigoryev, S. A., G. Arya, …, T. Schlick. 2009. Evidence for heteromorphic chromatin fibers from analysis of nucleosome interactions. *Proc. Natl. Acad. Sci. USA.* 106:13317–13322.
23. Sun, J., Q. Zhang, and T. Schlick. 2005. Electrostatic mechanism of nucleosomal array folding revealed by computer simulation. *Proc. Natl. Acad. Sci. USA.* 102:8180–8185.
24. Mergell, B., R. Everaers, and H. Schiessel. 2004. Nucleosome interactions in chromatin: fiber stiffening and hairpin formation. *Phys. Rev. E Stat. Nonlin. Soft Matter Phys.* 70:011915.
25. Stehr, R., N. Kepper, …, G. Wedemann. 2008. The effect of internucleosomal interaction on folding of the chromatin fiber. *Biophys. J.* 95:3677–3691.

26. Gerchman, S. E., and V. Ramakrishnan. 1987. Chromatin higher-order structure studied by neutron scattering and scanning transmission electron microscopy. *Proc. Natl. Acad. Sci. USA.* 84:7802–7806.

27. Kobori, T., S. Iwamoto, …, T. Ohtani. 2007. Chromatin dynamics of unfolding and refolding controlled by the nucleosome repeat length and the linker and core histones. *Biopolymers.* 85:295–307.

28. Hammermann, M., K. Tóth, …, J. Langowski. 2000. Salt-dependent compaction of di- and trinucleosomes studied by small-angle neutron scattering. *Biophys. J.* 79:584–594.

29. Draves, P. H., P. T. Lowary, and J. Widom. 1992. Co-operative binding of the globular domain of histone H5 to DNA. *J. Mol. Biol.* 225: 1105–1121.

30. Thomas, J. O., C. Rees, and J. T. Finch. 1992. Cooperative binding of the globular domains of histones H1 and H5 to DNA. *Nucleic Acids Res.* 20:187–194.

31. Woodcock, C. L., S. A. Grigoryev, …, N. Whitaker. 1993. A chromatin folding model that incorporates linker variability generates fibers resembling the native structures. *Proc. Natl. Acad. Sci. USA.* 90:9021–9025.

32. Barbi, M., J. Mozziconacci, and J. M. Victor. 2005. How the chromatin fiber deals with topological constraints. *Phys. Rev. E Stat. Nonlin. Soft Matter Phys.* 71:031910.

33. Diesinger, P. M., and D. W. Heermann. 2005. The two-angle model and the phase diagram for chromatin. *Phys. Rev. E Stat. Nonlin. Soft Matter Phys.* 74:031904–031912.

34. Diesinger, P. M., and D. W. Heermann. 2008. The influence of the cylindrical shape of the nucleosomes and H1 defects on properties of chromatin. *Biophys. J.* 94:4165–4172.

35. Schiessel, H., W. M. Gelbart, and R. Bruinsma. 2001. DNA folding: structural and mechanical properties of the two-angle model for chromatin. *Biophys. J.* 80:1940–1956.

36. Bešker, N., C. Anselmib, and P. D. Santis. 2004. Theoretical models of possible compact nucleosome structures. *Biophys. Chem.* 115:139–143.

37. Depken, M., and H. Schiessel. 2009. Nucleosome shape dictates chromatin fiber structure. *Biophys. J.* 96:777–784.

38. Livolant, F., S. Mangenot, …, D. Durand. 2006. Are liquid crystalline properties of nucleosomes involved in chromosome structure and dynamics? *Philos. Transact. A Math. Phys. Eng. Sci.* 364:2615–2633.

39. Woodcock, C. L. 2006. Chromatin architecture. *Curr. Opin. Struct. Biol.* 16:213–220.

40. Kruithof, M., F. Chien, …, J. van Noort. 2008. Subpiconewton dynamic force spectroscopy using magnetic tweezers. *Biophys. J.* 94:2343–2348.

41. Horowitz, R. A., D. A. Agard, …, C. L. Woodcock. 1994. The three-dimensional architecture of chromatin in situ: electron tomography reveals fibers composed of a continuously variable zig-zag nucleosomal ribbon. *J. Cell Biol.* 125:1–10.

42. Leuba, S. H., G. Yang, …, C. Bustamante. 1994. Three-dimensional structure of extended chromatin fibers as revealed by tapping-mode scanning force microscopy. *Proc. Natl. Acad. Sci. USA.* 91:11621–11625.

43. Wong, H., J.-M. Victor, and J. Mozziconacci. 2007. An all-atom model of the chromatin fiber containing linker histones reveals a versatile structure tuned by the nucleosomal repeat length. *PLoS One.* 2:e877.

44. Bishop, T. C., and J. E. Hearst. 1998. Potential function describing the folding of the 30 nm fiber. *J. Phys. Chem. B.* 102:6433–6439.

Biophysical Journal, Volume 98

Supporting Material

Exploring the conformational space of chromatin fibers and their stability by numerical dynamic phase diagrams

René Stehr, Robert Schöpflin, Ramona Ettig, Nick Kepper, Karsten Rippe, and Gero Wedemann

SUPPLEMENTARY MATERIALS

Exploring the conformational space of chromatin fibers and their stability by numerical dynamic phase diagrams

René Stehr[*], Robert Schöpflin[*], Ramona Ettig[†], Nick Kepper[†], Karsten Rippe[†], Gero Wedemann[*1]

[*] University of Applied Sciences Stralsund, System Engineering and Information Management, Zur Schwedenschanze 15, 18435 Stralsund, Germany

[†] Deutsches Krebsforschungszentrum & BIOQUANT, Research Group Genome Organization & Function, Im Neuenheimer Feld 280, 69120 Heidelberg, Germany

[1] to whom correspondence should be addressed: gero.wedemann@fh-stralsund.de

SUPPLEMENTARY METHODS

Representation of the chromatin chain in the six-angle model

As described in (1), the chromatin fiber is defined by a linear chain of segments, one for each nucleosome and two or three segments describing the intervening linker DNA. The position of the segment *i* in the chain is described by a position vector $\vec{p}_i$, while its orientation is described by a local coordinate system ($\vec{f}_i, \vec{u}_i, \vec{v}_i$) with $\vec{v}_i = \vec{u}_i \times \vec{f}_i$. The segment vector $\vec{s}_i$ is defined by $\vec{s}_i = \vec{p}_{i+1} - \vec{p}_i$ with the segment length $b_i = |\vec{s}_i|$ and $\vec{s}_i = \vec{u}_i \cdot b_i$. The geometrical center $\vec{m}_i$ of the nucleosome *i* is given by:

$$\vec{m}_i = \vec{p}_i + \frac{1}{2}\vec{s}_i + c \cdot \hat{a}_i, \qquad \text{(SM1)}$$

where *c* is the distance between the center of the segment and the nucleosome center, and $\hat{a}_i$ is the vector describing the direction from the segment center to the nucleosome center (Fig. SM1).

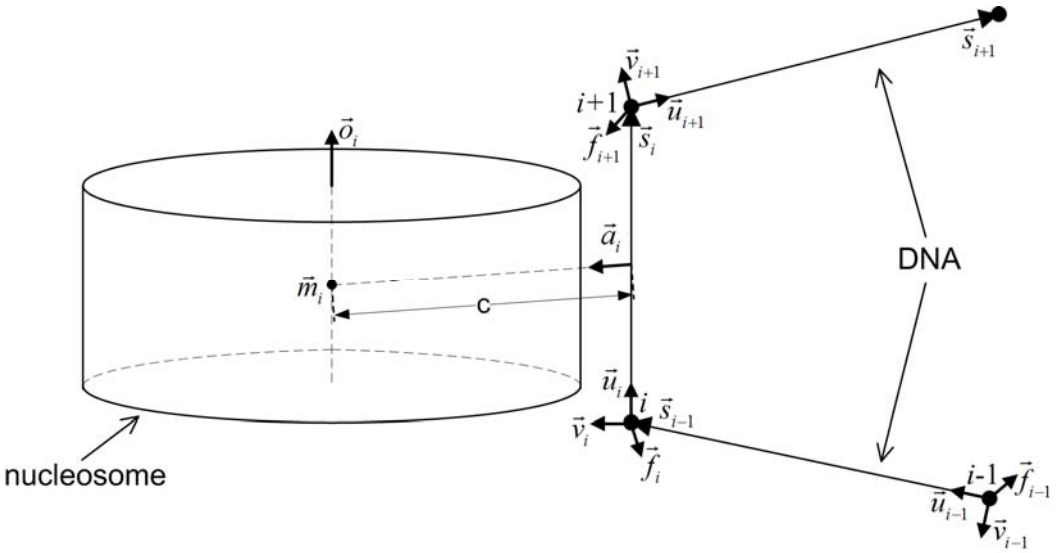

FIGURE SM1. Discretization of the chromatin fiber. Three segments are shown: *i* is the segment of the nucleosome, and *i*-1 and *i*+1 are segments of the incoming and outgoing linker DNA. For simplification, the shape of the nucleosome is shown as cylinder instead of a spherocylinder as it is used for the calculation of the internucleosomal interaction energy (see below).

In the previously used two-angle representation, for $\vec{a}_i$ and $\vec{o}_i$ holds: $\vec{a}_i = \vec{v}_i$ and $\vec{o}_i = \vec{u}_i$ (1). Thus, the orientation of the nucleosome was parallel to the segment vector and the center was situated symmetrically with respect to the segment vector. In contrast, in the six-angle model the nucleosome center and orientation can be shifted and rotated relative to the segment vector (2). Therefore, $\vec{a}_i$ is defined by two rotations of the vector $\vec{v}_i$: around $\vec{u}_i$ by the angle ε and around $\vec{f}_i$ by the angle ϕ (2) (Figs. 1 *A* and SM1). Similarly, $\vec{o}_i$ is described by two rotations of the vector $\vec{u}_i$: around $\vec{v}_i$ by the angle δ and around $\vec{f}_i$ by the angle ζ (Figs. 1 *A* and SM1). Note that ζ is not included in former descriptions of the six-angle model, since it has not been needed for the description of fiber conformations studied. The nucleosome description of the six-angle model (2) is compatible with the description of the two-angle model (1) if the angles ε, ϕ, δ and ζ are set to 0°. For more details see Fig. 1 *A* and the corresponding text.

Elastic energies

The elastic interactions described in (1) are assumed to be harmonic. The strength constants of the interactions are named $a_{(Y)}^{(X)}$ in which X denotes the type of interaction. This can be stretching (s), bending (b) or torsion (t). The interaction partners are denoted by Y, which can be either DNA or nucleosome. The stretching energy is defined by:

$$U_{Stretch} = \frac{a_Y^{(s)}}{b_i^0}\left(b_i - b_i^0\right)^2, \qquad \text{(SM2)}$$

with b_i is the current length of the segment as described above and b_i^0 is the equilibrium length of the segment. The equilibrium length is defined by the chosen DNA linker length divided by the number of segments between adjacent nucleosomes. For nucleosomes, b_i^0 is defined as the equilibrium distance *d* between incoming and outgoing DNA (Fig. 1 *A*).

For the bending energy, an equilibrium nucleosome geometry is defined by the incoming and outgoing linker DNA. The bending angle is computed between the segment vector $\vec{u}_{i+1}$ and its equilibrium direction $\vec{B}_i$ relative to the connected segment. $\vec{B}_i$ is defined by the angles ω_i and ξ_i:

$$\vec{B}_i = \vec{f}_i \sin\omega_i \cos\xi_i + \vec{v}_i \sin\omega_i \sin\xi_i + \vec{u}_i \cos\omega_i \qquad \text{(SM3)}$$

and the bending angle θ_i is calculated from $\cos(\theta_i) = \vec{B}_i \vec{u}_{i+1}$. The bending energy is given by:

$$U_{Bend} = \frac{a_Y^{(b)}}{b_i^0}\theta_i^2 \qquad \text{(SM4)}$$

The angles ω_i and ξ_i for the intrinsic bending of two segments i and i+1 are defined by the parameters α and γ of the six-angle model (Fig. 1 *A*):

$$\xi_i = \begin{cases} (\pi-\alpha)/2 & ,if\ i \in NUC \wedge i+1 \in DNA \\ \pi/2 & ,if\ i \in DNA \wedge i+1 \in NUC \\ 0 & ,if\ i \in DNA \wedge i+1 \in DNA \end{cases} \qquad \text{(SM5)}$$

$$\omega_i = \begin{cases} (-\pi+\gamma)/2 & ,if\ i \in NUC \wedge i+1 \in DNA \\ (-\pi+\gamma)/2 & ,if\ i \in DNA \wedge i+1 \in NUC \\ 0 & ,if\ i \in DNA \wedge i+1 \in DNA \end{cases} \qquad \text{(SM6)}$$

In the two-angle model (1), the equilibrium entry-exit angle of the DNA at the nucleosome was defined by α measured parallel to the flat side of the nucleosome cylinder. In the six-angle model, the additional angle γ describes the entry-exit-angle measured perpendicular to the flat side of the nucleosome cylinder (Fig. 1 *A*). If γ = 0°, the equilibrium position of the six-angle model (Eqs. SM5 and SM6) corresponds to the two-angle model.

For the torsion energy, an intrinsic torsion is considered. The coordinate systems of two connected segments i and i+1 can be mapped on each other by an Euler-transformation with the angles (α_i, β_i, γ_i) in which the rotation of the first angle is around $\vec{u}_i$. Then $\alpha_i + \gamma_i - \tau_i$ is the total torsion with τ_i is the intrinsic torsion. The torsion potential is then:

$$U_{Torsion} = \frac{a_Y^{(t)}}{b_i^0}\left(\alpha_i + \gamma_i - \tau_i\right)^2 \qquad \text{(SM7)}$$

The intrinsic torsion τ_i of two segments i and i+1 is defined by the parameters α and β of the two- and six-angle model (Fig. 1 *A*):

$$\tau_i = \begin{cases} \beta - \pi - \alpha/2 & ,if\ i \in NUC \wedge i+1 \in DNA \\ -\alpha/2 & ,if\ i \in DNA \wedge i+1 \in NUC \\ 0 & ,if\ i \in DNA \wedge i+1 \in DNA \end{cases} \qquad \text{(SM8)}$$

Electrostatic Energy

The electrostatic interaction between DNA segments is determined by integrating the solution of the Debye-Hückel equation for a point charge over two charged line segments (1):

$$E_{ij}^{(e)} = \frac{\nu^2}{D} \int d\lambda_i \int d\lambda_j \frac{\exp(-\kappa r_{ij})}{r_{ij}} \qquad \text{(SM9)}$$

D is the dielectric constant of water, and κ the inverse of the Debye length. r_{ij} is the distance between the current positions at the segments i and j to which the integration parameters λ_i, λ_j correspond. The charge per unit length ν is chosen such that the potential at the radius of the DNA coincides with the solution of the Poisson-Boltzmann equation for a cylinder with charge per length ν_0^*. For DNA in the presence of the Gouy layer of immobile counterions, this can be computed as $\nu_0^* = q\nu_0$ in which $\nu_0 = -2e/\Delta$ is the charge per length of the naked DNA (3), e is the proton charge, and Δ = 0.34 nm is the distance between base pairs. Following Stigter, the value of q is 0.73 (4). To save computation time, a tabulation of the double integral is used. The table is parameterized by the distance of the segments and three values describing its relative orientation. During the simulation a linear interpolation of the tabulated values was used.

Internucleosomal potential

The anisotropic internucleosomal interaction is described by a series expansion in S-functions (5). This potential is based on the 12-6 Lennard-Jones potential:

$$U(\hat{o}_1,\hat{o}_2,\vec{r}) = 4\varepsilon(\hat{o}_1,\hat{o}_2,\hat{r})\left[\left(\frac{\sigma_0}{|\vec{r}|-\sigma(\hat{o}_1,\hat{o}_2,\hat{r})+\sigma_0}\right)^{12}-\left(\frac{\sigma_0}{|\vec{r}|-\sigma(\hat{o}_1,\hat{o}_2,\hat{r})+\sigma_0}\right)^{6}\right], \quad \text{(SM10)}$$

with $\hat{o}_1$ and $\hat{o}_2$ as unit vectors defining the orientation of the particles (see above), $\vec{r}$ as the vector of the distance of the particles ($\vec{r} = \vec{m}_2 - \vec{m}_1$) and σ_0 scales the potential width. The potential strength (ε) and range (σ) parameters depend on the orientation and center-to-center difference vectors of two nucleosomes and define the anisotropy of the potential. For the Zewdie potential, the two factors were described by S-functions for identical cylindrically symmetric particles (6, 7). The potential range is defined as:

$$\sigma(\hat{o}_1,\hat{o},\hat{r}) = \sigma_0[\sigma_{000}S_{000} + \sigma_{cc2}(S_{202}+S_{022}) + \sigma_{220}S_{220} + \sigma_{222}S_{222} + \sigma_{224}S_{224}], \quad \text{(SM11)}$$

and the potential strength is given by:

$$\varepsilon(\hat{o}_1,\hat{o}_2,\hat{r}) = \varepsilon_0[\varepsilon_{000}S_{000} + \varepsilon_{cc2}(S_{202}+S_{022}) + \varepsilon_{220}S_{220} + \varepsilon_{222}S_{222} + \varepsilon_{224}S_{224}], \quad \text{(SM12)}$$

where ε_0 is the maximum potential strength. The S-functions (S_{000}, S_{202}, S_{022}, S_{220}, S_{222} and S_{224}) depend on the orientation of the nucleosomes and the difference vector between the nucleosome centers. They are listed in Table SM1. The expansion coefficients for the strength (ε_{000}, ε_{cc2}, ε_{220}, ε_{222}, ε_{224}) and range (σ_{000}, σ_{cc2}, σ_{220}, σ_{222}, σ_{224}) are responsible for the dimension of the nucleosome shape and for the ratio of the energy strength between different oriented nucleosomes (e.g., top-on-top and side-by-side), respectively. While the range coefficients were chosen in order to fit the dimensions of the nucleosome (width = 11 nm and height = 5.5 nm), the strength expansion coefficients were chosen to achieve a ratio of 1/12 between side-by-side and top-on-top oriented nucleosomes (5). The actual values for these coefficients as well as for the range parameter were determined by performing least square fits (5) and are shown in Table SM2.

TABLE SM1. The first six S-functions for identical cylindrically symmetric particles. $\hat{o}_1$ and $\hat{o}_2$ are the unit vectors defining the orientation of the particles (Fig. SM1) and $\hat{r}$ is the unit vector of the center-to-center distance of the particles.

$f_0 = \hat{o}_1 \cdot \hat{o}_2$, $f_1 = \hat{o}_1 \cdot \hat{r}$, $f_2 = \hat{o}_2 \cdot \hat{r}$.
$S_{000} = 1$, $S_{202} = (3f_1^{\,2} - 1)/2\sqrt{5}$, $S_{022} = (3f_2^{\,2} - 1)/2\sqrt{5}$, $S_{220} = (3f_0^{\,2} - 1)/2\sqrt{5}$,
$S_{222} = (2 - 3f_1^2 - 3f_2^2 - 3f_0^2 + 9f_1 f_2 f_0)/\sqrt{70}$,
$S_{224} = (1 + 2f_0^2 - 5f_1^2 - 5f_2^2 - 20f_0 f_1 f_2 + 35f_1^2 f_2^2)/4\sqrt{70}$

TABLE SM2. Parameters of the nucleosome-nucleosome potential for the ratio $E_{lateral}/E_{longitudinal}$ = 1/12 between the maximum interaction energy of lateral and longitudinal oriented nucleosomes.

Parameter	**Value**
S000	1.6957
Scc2	-0.7641
S220	-0.1480
S222	-0.2582
S224	0.5112
E000	2.7206
Ecc2	6.0995
E220	3.3826
E222	7.1036
E224	3.2870
σ_0	5.5 nm

In order to demonstrate the anisotropy of this potential, Fig. SM2 shows the energy of two nucleosomes in dependence of their distance and orientation for ε_0 = 0.5 k_BT (k_B is the Boltzmann constant and T is the temperature). It is apparent that for the top-on-top arrangement the highest attraction energy $E_{\max}$ appears, which corresponds to $12 \cdot \varepsilon_0$ (14.6 kJ/mol), while the side-by-side arranged nucleosomes lead to a maximum attraction energy of ε_0 (1.2 kJ/mol).

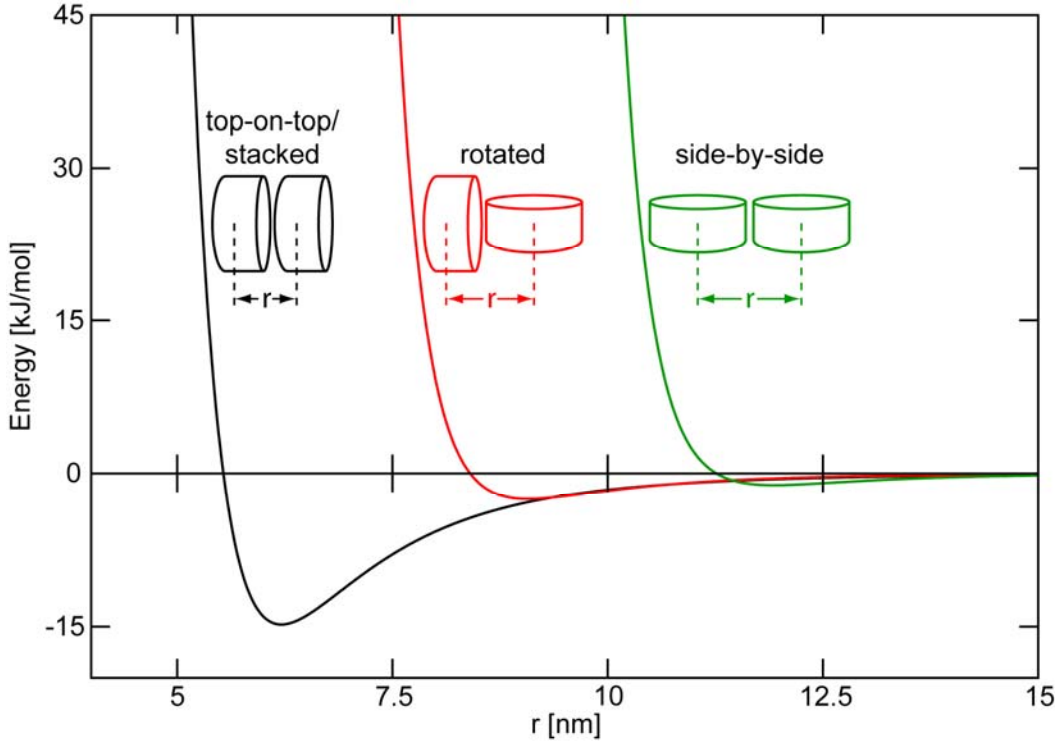

FIGURE SM2. Zewdie-Potential as function of the center-to-center distances r for different oriented nucleosome pairs. The parameters of the potential are shown in Table SM2. The maximum potential depth of top-on-top and side-by-side arranged nucleosomes deviates by the factor 12. For all curves, the energy is zero at the distance where nucleosomes touch each other: $r_{top\text{-}on\text{-}top}$ = 5.5 nm, $r_{rotated}$ = 8.25 nm and $r_{side\text{-}by\text{-}side}$ = 11 nm.

DNA-Nucleosome excluded volume

In order to inhibit sterical overlaps between nucleosomes and linker DNA, a repulsive potential is defined. Therefore, the DNA is approximated by a number of overlapping spheres with the radius r_d = 1.2 nm corresponding to the DNA cylinder radius. Similar to the Zewdie potential, the nucleosome is represented as a spherocylinder with the particular condition that the radius and height are defined by r_n = 5.5 nm, which correspond to the nucleosome dimension (width = 11 nm and height = 5.5 nm) (Fig. SM3 *A*). The repulsion energy between a DNA linker and a nucleosome with the segment indices *D* and *N*, respectively, is defined by the summation of the interaction energy of each DNA-sphere with the nucleosome:

$$E_{DNA-Nuc} = \sum_{i=1}^{S} E'_{DNA-Nuc}\left(\vec{m}_N, \vec{o}_N, \vec{e}_{D,i}\right), \qquad \text{(SM 13)}$$

where S is the number of spheres per DNA segment, $\vec{m}_N$ and $\vec{o}_N$ are the center and orientation vectors of the nucleosome N (Fig. SM1), respectively, and $\vec{e}_{D,i}$ is the center of the ith sphere of the DNA segment D:

$$\vec{e}_{D,i} = \vec{p}_D + \vec{s}_D \cdot r_d + (i-1)\frac{b_D - 2r_d}{S-1}\vec{s}_D . \qquad \text{(SM 14)}$$

As described above, $\vec{s}_D$ is the segment D, $\vec{p}_D$ is the starting point of the segment, and b_D is the length of the segment (Fig. SM1). The energy $E'_{DNA-Nuc}$ of one DNA-sphere and a nucleosome is defined by:

$$E'_{DNA-Nuc}(\vec{m},\vec{o},\vec{e}) = \begin{cases} 0, & \text{if } d(\vec{m},\vec{o},\vec{e}) \geq r_n + r_d \\ k \cdot \left(d(\vec{m},\vec{o},\vec{e}) - r_n - r_d\right)^{12}, & else \end{cases} , \qquad \text{(SM 15)}$$

with k is the energy scaling constant. The parameter $d(\vec{m},\vec{o},\vec{e})$ defines the minimum distance between the center of the DNA sphere $\vec{e}$ and the nucleosome center axis, which is defined by the center $\vec{m}$ and the orientation $\vec{o}$ of the nucleosome (Fig. SM1). The distance $d(\vec{m},\vec{o},\vec{e})$ is computed from the projection of the DNA-sphere center on the plane of the nucleosome center axis. Accordingly, the vector $\vec{n}$ defines the projection point of the DNA-sphere center on the plane of the nucleosome center axis (Fig. SM3 *B*):

$$\vec{n} = \vec{e} - \left(\hat{o} \cdot (\vec{e} - \vec{m})\right) \cdot \hat{o} , \qquad \text{(SM 16)}$$

and the vector $\vec{q} = \vec{n} - \vec{m}$ is the distance between this point and the nucleosome center. Thus, the distance $d(\vec{m},\vec{o},\vec{e})$ is calculated by:

$$d(\vec{m},\vec{o},\vec{e}) = \begin{cases} \left|\vec{e} - \vec{n}\right|, & if \ \left|\vec{q}\right| < r_n / 2 \\ \left|\vec{e} - \left(\vec{m} + \frac{r_n}{2} \cdot \hat{q}\right)\right|, & else \end{cases} . \qquad \text{(SM17)}$$

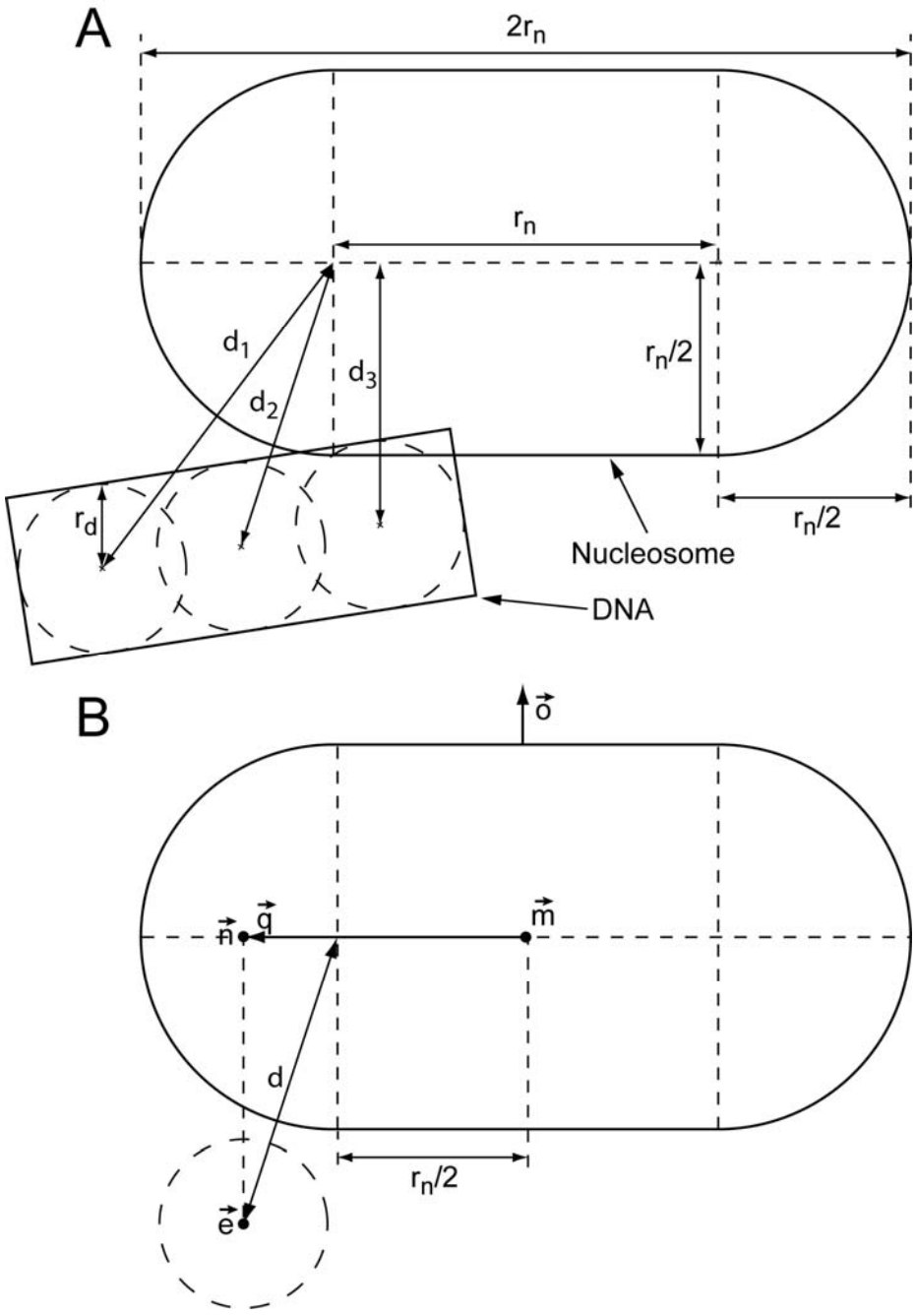

FIGURE SM3. Schematic representation of the DNA-nucleosome excluded volume. (A) The nucleosome is represented as spherocylinder with the radius and height r_n, while the DNA cylinder is approximated by a number of spheres, in this case three, with the radius r_d. The distances d_1, d_2 and d_3 indicate the minimum distances between the nucleosome center axis and the DNA spheres. An overlap occurs if $d < r_d + r_n$. In this example, the third sphere exhibits an overlap since $d_3 < r_d + r_n$. (B) The distance d between a DNA-sphere and the nucleosome is computed by the projection point $\vec{n}$ of the DNA-sphere center $\vec{e}$ on the plane of the nucleosome center axis (Eq. SM16). If the length of the vector $\vec{q}$ is smaller than $r_n/2$, then d is the distance between $\vec{e}$ and $\vec{n}$, otherwise d is defined by the distance between $\vec{e}$ and $\vec{m} + \hat{q} \cdot r_n/2$ (Eq. SM 17).

SUPPLEMENTARY TABLES

TABLE S1. Parameters used in the MC simulations. The elastic parameters were chosen as described by Wedemann and Langowski (1). For the DNA, the values are based on the average of experimentally determined values of 45 - 50 nm DNA bending persistence length and a DNA torsion elasticity of $2.8 \pm 0.2 \cdot 10^{-19}$ J nm (8). The elasticity of the nucleosome/chromatosome has not been derived from experimental studies. Therefore, values were chosen that essentially maintain the initial conformation of the chromatosome.

Parameter	Value
Stretching module DNA	$1.10 \cdot 10^{-18}$ J nm
Bending module DNA	$2.06 \cdot 10^{-19}$ J nm
Torsion module DNA	$2.67 \cdot 10^{-19}$ J nm
Electrostatic radius DNA	1.2 nm
Stretching module nucleosome	$1.10 \cdot 10^{-18}$ J nm
Torsion module nucleosome	$1.30 \cdot 10^{-18}$ J nm
Temperature	293 K
Ionic strength	100 mM NaCl

Table S2. Six-angle model geometries and properties for different chromatin fiber models. The CL and ID structures were developed in (2) and the CLS geometry in (5). The diameter and linear mass density were computed from the statistical ensemble in thermal equilibrium. The ID geometry with NRL > 187 bp did not lead to an obvious nucleosome stacking pattern, and structures with NRL = 207 bp did not form fiber-like structures in thermal equilibrium (2).

Geometry	**NRL** (bp)	ψ (°)	α (°)	γ (°)	β (°)	ε (°)	ϕ (°)	δ (°)	c (nm)	d (nm)	**Fiber Type** [N_{stack}, N_{step}]	**diameter** (nm)	**linear mass density** (nucleosomes/11 nm fiber)
CL	169	70	50	-50	220	0	0	20	3.3	8	[2, 1]	26.2 ± 0.2	3.1 ± 0.1
CLS	212	26	26	0	260	0	0	0	8	3.1	[3, 1]	36 ± 0.7	4.6 ± 0.1
ID	187	128	117.5	-65	0	0	0	60	5.6	3.7	[6, 1]	30.1 ± 0.1	7.6 ± 0.2
ID	197	121	117.5	-39	0	0	0	58	5.6	3.7	—	37.5 ± 0.4	6.9 ± 0.5
ID	207	120	117.5	-28	0	0	0	52	5.6	3.7	—	—	—

TABLE S3. Energies of simulated chromatin structures at different simulation steps. The remaining parameters of the six-angle model correspond to the descriptions of Table S2. For each system, the energy for three stages of the simulations is shown: i) before simulation corresponding to the values of the static phase diagrams (static PD), ii) after 10^7 Monte Carlo (MC) steps corresponding to the dynamic phase diagrams (dynamic PD), and iii) the mean value for the simulated structure in thermal equilibrium. The differences between the energies of simulated structures after 10^7 MC steps (dynamic PD) and the mean values in thermal equilibrium are marginal.

Geometry	**NRL** (bp)	ψ (°)	α (°)	γ (°)	β (°)	**energy static PD** (k_BT)	**energy dynamic PD** (k_BT)	**mean energy thermal equilibrium** (k_BT)
former models (see refs.(2, 5), Fig. S1 and Table S2)								
CL	169	70	50	-50	220	197078	383	426 ± 28
CLS	212	26	26	0	260	106601	369	361 ± 28
ID	187	128	117.5	-65	0	35450	99	98 ± 28
ID	197	121	117.5	-39	0	239	168	138 ± 31
ID	207	120	117.5	-28	0	1114	312	320 ± 32
new models (see Fig. 5 and Table 1)								
CL	169	25	17.7	-17.7	175	201991	208	290 ± 35
ID	187	117.5	117.5	0	295	96882	21	55 ± 28
ID	187	125	117.5	-54.23	355	94898	46	88 ± 28
ID	197	130	117.5	-70.89	355	-75	14	89 ± 27

SUPPLEMENTARY FIGURES

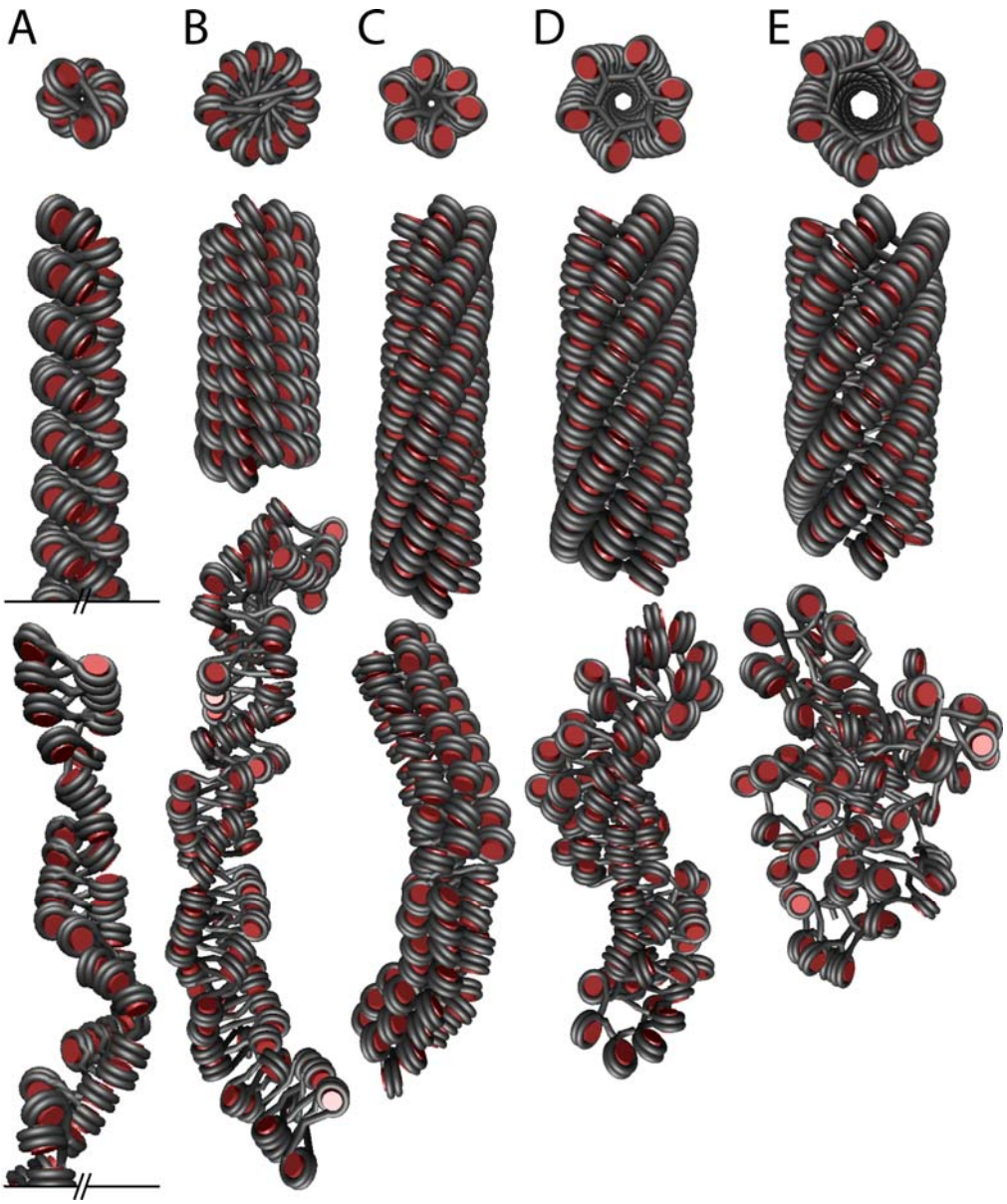

FIGURE S1. Chromatin fiber models for different nucleosome geometries. The configurations were generated by MC simulations. The simulated fibers are designated according to the denotation of Depken and Schiessel (9) (Fig. 1 *B*). (A) Crossed-linker (CL) geometry derived from the tetranucleosome crystal-structure (2) lead to a [2, 1] fiber. (B) Crossed-linker model with nucleosome stem (CLS) for native chromatin of chicken erythrocytes (5) lead to a partially broken [3, 1] fiber. (C, D, E) Interdigitated geometry (ID) including linker histones with NRL of 187, 197 and 207 bp, respectively. These models were developed to reproduce the experimental data of reconstituted chromatin fibers with high mass densities (2). For an NRL of 187 bp, a [6, 1] fiber is obtained (C), while for higher NRLs (D and E) no uniform nucleosome stacking occurred.

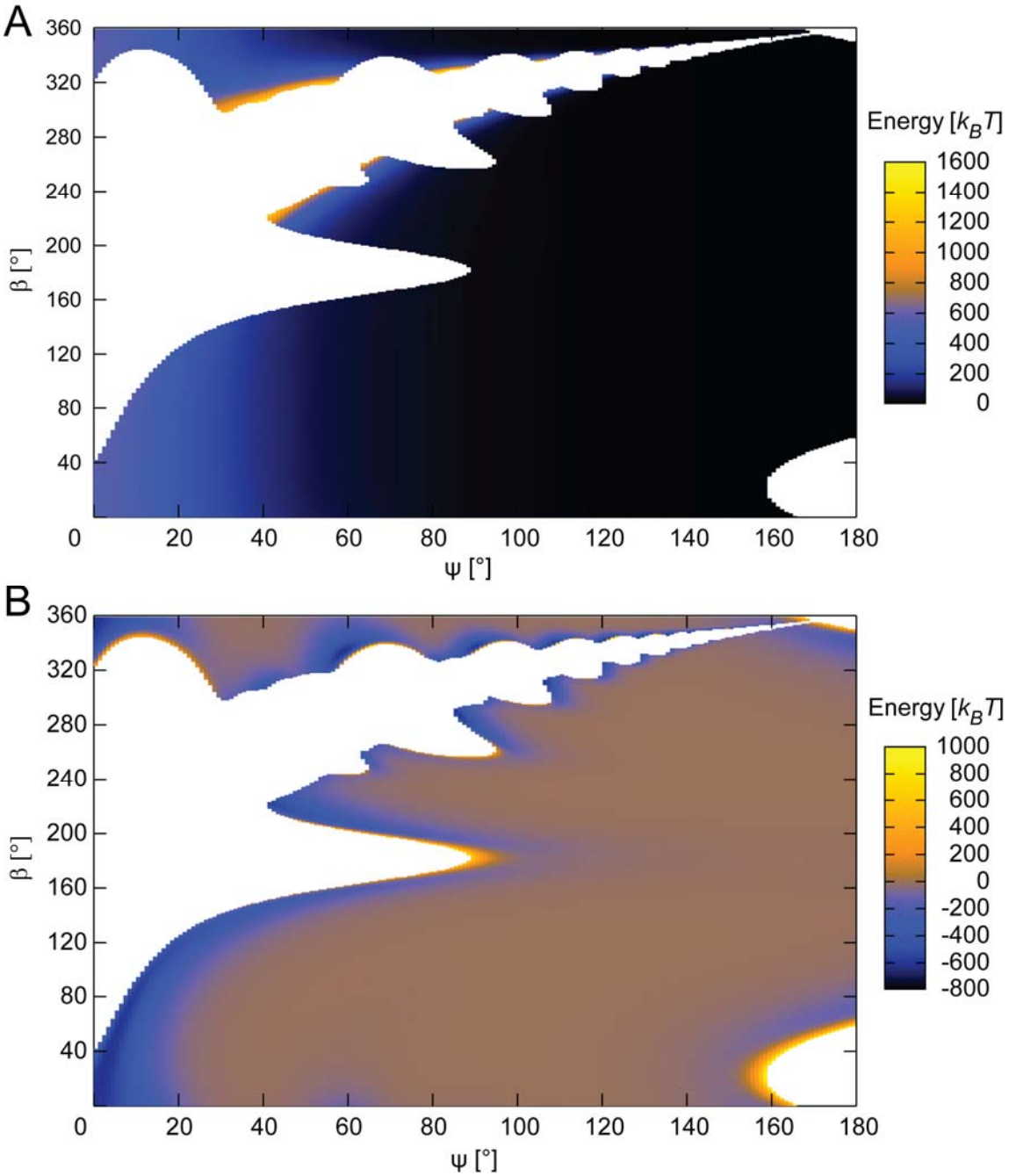

FIGURE S2. Static phase diagrams of single energies of the CLS geometry with NRL = 212 bp for the opening angle ψ ($\gamma = 0$) and the nucleosome twist angle β with a step width of 1°. The corresponding phase diagram of the total energy is shown in Fig. 2 *B*. (A) Electrostatic energy of the linker DNA segments. The highest energies occur at the border between sterically possible and impossible conformations. However, there are also borders with very low electrostatic energy. (B) Energy of the nucleosome-nucleosome interaction. The lowest energy appears near the border between sterically possible and impossible conformations.

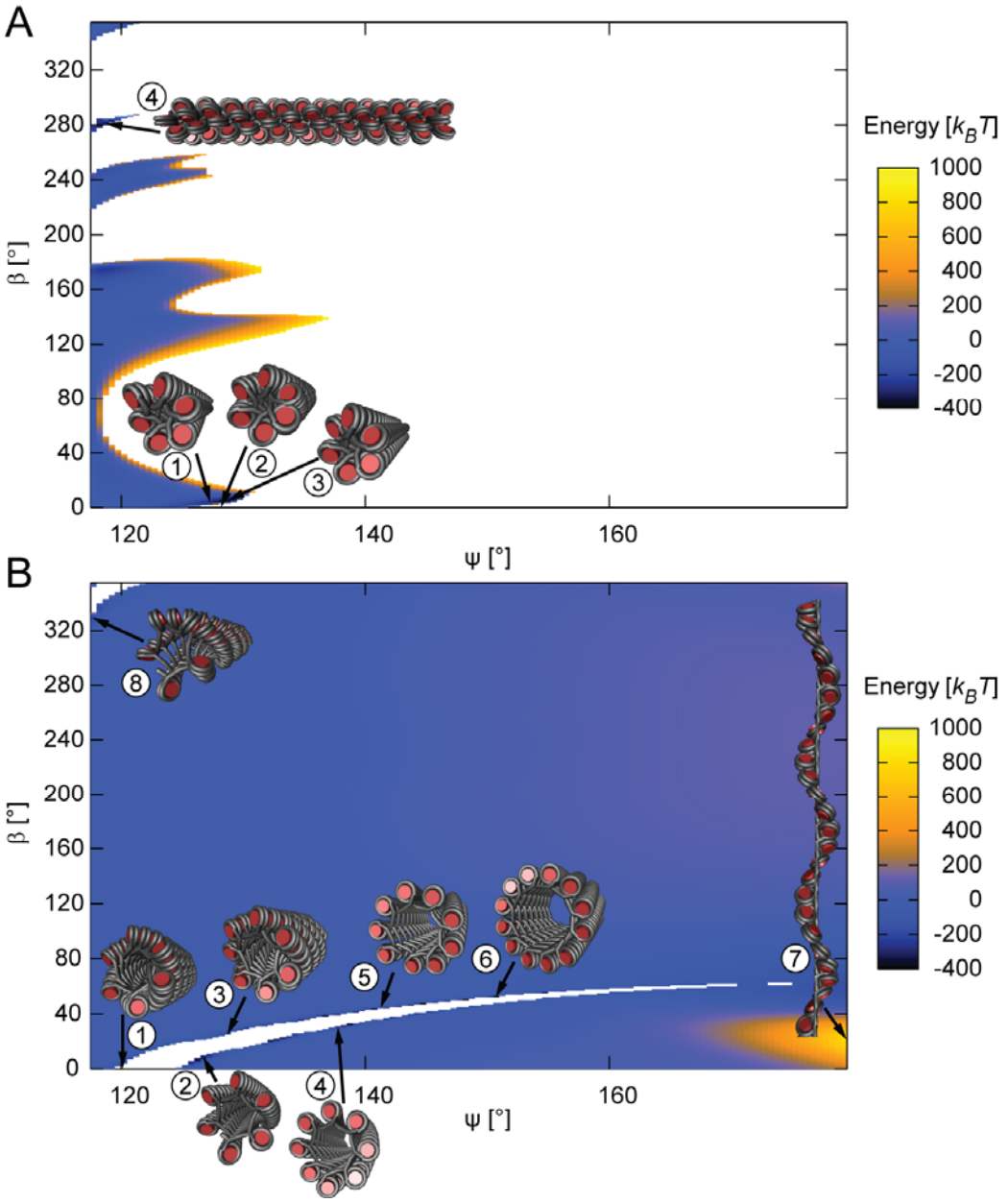

FIGURE S3. Energy phase diagrams for the ID geometry. A value of α = 117.5° was used, while γ was varied in order to reach the indicated value of the opening angle ψ. Step widths of 0.5° and 1° were used for ψ and β, respectively. Fibers with the lowest energy were found at the border between sterically possible and impossible conformations. Previous models for reconstituted chromatin fibers in the elastically relaxed state are located in sterically forbidden areas (A: fiber 2, B: fiber 1). (A) NRL = 187 bp. Broad energy valleys are apparent for two fiber types: [6, 1] fibers with nucleosomes perpendicular to the fiber axis (fibers 1 and 3), and fibers with nucleosomes parallel to the fiber axis with no apparent nucleosome stacking (fiber 4). (B) NRL = 207 bp. No obvious energy valleys exist but fibers with a high number of nucleosome stacks and large diameter had the lowest energies (fibers 2-6 and 8). These interdigitated fibers can be described by [n, 1] where n is the number of nucleosome stacks in the range of 5 (fiber 8), 12 (fiber 6) and above for higher ψ values (fibers not shown).

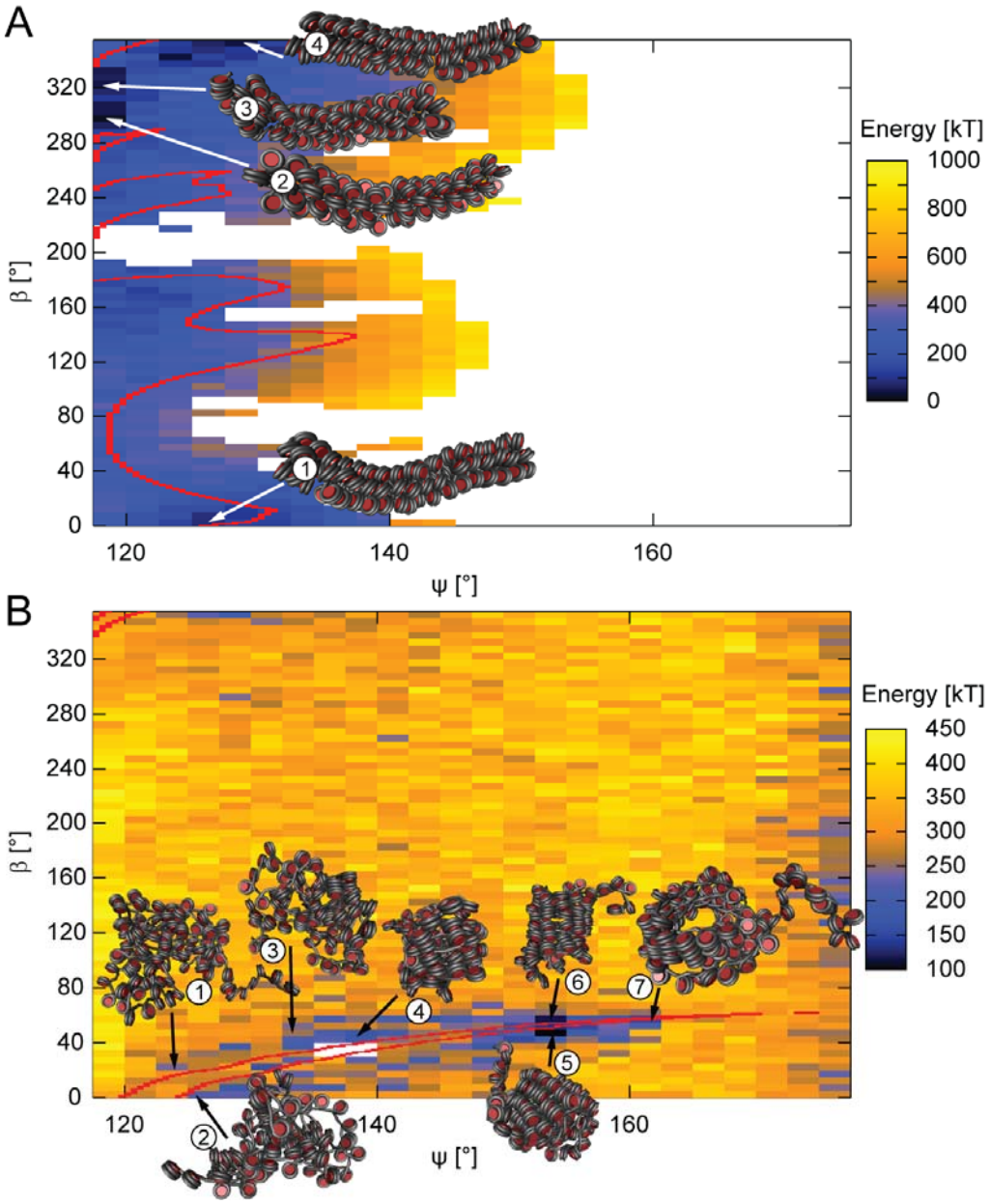

FIGURE S4. Dynamic energy phase diagrams of the ID geometry for the opening angle ψ and the nucleosome twist angle β. Simulations for 10^7 MC steps were conducted and the last configurations of the simulated trajectories were used for analysis. The red contour lines indicate the former borderline between the sterically possible and impossible conformations of the static phase diagrams (Fig. S3). For both NRLs, the chromatin structures became more irregular and the region of the sterically forbidden area reduced significantly. (A) NRL = 187 bp. Two different structures are energetically most favorable: ID fibers with nucleosomes parallel to the fiber axis, e.g., fiber 2 with no apparent nucleosome stacking, and fibers with nucleosomes perpendicular to the fiber axis, e.g., [5, 1] (fiber 3) and [6, 1] (fibers 1 and 4) fiber conformations. (B) NRL = 207 bp. Most of the chromatin fibers did not retain their initial conformation during the simulations (fibers 1-4). Only fibers with a high number of nucleosome stacks (> 11) and high diameters (> 47 nm) converged to stable fiber-like structures, e.g., fiber 5: [12, 1], fiber 6: [13, 1], and fiber 7: [17, 1].

REFERENCES

1. Wedemann, G., and J. Langowski. 2002. Computer simulation of the 30-nanometer chromatin fiber. Biophys J 82:2847-2859.
2. Kepper, N., D. Foethke, R. Stehr, G. Wedemann, and K. Rippe. 2008. Nucleosome geometry and internucleosomal interactions control the chromatin fiber conformation. Biophys J 95:3692-3705.
3. Schellman, J., and D. Stigter. 1977. Electrical double layer, zeta potential, and electrophoretic charge of double stranded DNA. Biopolymers 16:1415–1434.
4. Stigter, D. 1977. Interactions of highly charged colloidal cylinders with applications to double stranded DNA. Biopolymers 16:1435–1448.
5. Stehr, R., N. Kepper, K. Rippe, and G. Wedemann. 2008. The Effect of Internucleosomal Interaction on Folding of the Chromatin Fiber. Biophys J 95:3677-3691.
6. Stone, A. J. 1978. The description of bimolecular potentials, forces and torques: the S and V function expansions. Molec. Phys. 36:241–256.
7. Zewdie, H. 1998. Computer-simulation studies of diskotic liquid crystals. PHYSICAL REVIEW E 57:1793-1805.
8. Bloomfield, V. A., D. M. Crothers, and I. Tinocco. 2000. Nucleic Acids Structures, Properties, and Functions. University Science Books.
9. Depken, M., and H. Schiessel. 2009. Nucleosome shape dictates chromatin-fiber structure. Biophys J 96:777–784.